Dear Author,

Here are the proofs of your article.

- You can submit your corrections **online**, via **e-mail** or by **fax**.
- For **online** submission please insert your corrections in the online correction form. Always indicate the line number to which the correction refers.
- You can also insert your corrections in the proof PDF and **email** the annotated PDF.
- For fax submission, please ensure that your corrections are clearly legible. Use a fine black pen and write the correction in the margin, not too close to the edge of the page.
- Remember to note the **journal title**, **article number**, and **your name** when sending your response via e-mail or fax.
- **Check** the metadata sheet to make sure that the header information, especially author names and the corresponding affiliations are correctly shown.
- **Check** the questions that may have arisen during copy editing and insert your answers/ corrections.
- **Check** that the text is complete and that all figures, tables and their legends are included. Also check the accuracy of special characters, equations, and electronic supplementary material if applicable. If necessary refer to the *Edited manuscript.*
- The publication of inaccurate data such as dosages and units can have serious consequences. Please take particular care that all such details are correct.
- Please **do not** make changes that involve only matters of style. We have generally introduced forms that follow the journal's style. Substantial changes in content, e.g., new results, corrected values, title and authorship are not allowed without the approval of the responsible editor. In such a case, please contact the Editorial Office and return his/her consent together with the proof.
- If we do not receive your corrections **within 48 hours**, we will send you a reminder.
- Your article will be published **Online First** approximately one week after receipt of your corrected proofs. This is the **official first publication** citable with the DOI. **Further changes are, therefore, not possible.**
- The **printed version** will follow in a forthcoming issue.

Please note

After online publication, subscribers (personal/institutional) to this journal will have access to the complete article via the DOI using the URL: http://dx.doi.org/[DOI].
If you would like to know when your article has been published online, take advantage of our free alert service. For registration and further information go to: http://www.link.springer.com.

Due to the electronic nature of the procedure, the manuscript and the original figures will only be returned to you on special request. When you return your corrections, please inform us if you would like to have these documents returned.

Metadata of the article that will be visualized in OnlineFirst

ArticleTitle	Low-dimensional models of single neurons: a review	
Article Sub-Title		
Article CopyRight	The Author(s), under exclusive licence to Springer-Verlag GmbH Germany, part of Springer Nature (This will be the copyright line in the final PDF)	
Journal Name	Biological Cybernetics	
Corresponding Author	FamilyName	**Rotstein**
	Particle	
	Given Name	**Horacio G.**
	Suffix	
	Division	Federated Department of Biological Sciences
	Organization	New Jersey Institute of Technology and Rutgers University
	Address	Newark, USA
	Phone	
	Fax	
	Email	horacio@njit.edu
	URL	
	ORCID	
Author	FamilyName	**Chialva**
	Particle	
	Given Name	**Ulises**
	Suffix	
	Division	Departamento de Matemática
	Organization	Universidad Nacional del Sur and CONICET
	Address	Bahía Blanca, Argentina
	Phone	
	Fax	
	Email	
	URL	
	ORCID	
Author	FamilyName	**Boscá**
	Particle	
	Given Name	**Vicente González**
	Suffix	
	Division	Courant Institute of Mathematical Sciences
	Organization	New York University
	Address	New York, USA
	Phone	
	Fax	
	Email	
	URL	
	ORCID	
Schedule	Received	13 Nov 2022
	Revised	
	Accepted	5 Mar 2023
Abstract	The classical Hodgkin–Huxley (HH) point-neuron model of action potential generation is four-dimensional. It consists of four ordinary differential equations describing the dynamics of the membrane potential and three gating variables associated to a transient sodium and a delayed-rectifier potassium ionic currents. Conductance-based models of HH type are higher-dimensional extensions of the classical HH model. They include a number of supplementary state variables associated with other ionic current types, and are able to describe additional phenomena such as subthreshold oscillations, mixed-mode oscillations (subthreshold oscillations interspersed with spikes), clustering and bursting. In this manuscript we discuss biophysically plausible and phenomenological reduced models that preserve the biophysical and/or dynamic description of models of HH type and the ability to produce complex phenomena, but the number of effective dimensions (state variables) is lower. We describe several representative models. We also describe systematic and heuristic methods of deriving reduced models from models of HH type.	
Footnote Information	Communicated by Benjamin Lindner.	

Biological Cybernetics
https://doi.org/10.1007/s00422-023-00960-1

Biological Cybernetics

REVIEW ARTICLE

Low-dimensional models of single neurons: a review

Ulises Chialva[1] · Vicente González Boscá[2] · Horacio G. Rotstein[3]

Received: 13 November 2022 / Accepted: 5 March 2023

Abstract

The classical Hodgkin–Huxley (HH) point-neuron model of action potential generation is four-dimensional. It consists of four ordinary differential equations describing the dynamics of the membrane potential and three gating variables associated to a transient sodium and a delayed-rectifier potassium ionic currents. Conductance-based models of HH type are higher-dimensional extensions of the classical HH model. They include a number of supplementary state variables associated with other ionic current types, and are able to describe additional phenomena such as subthreshold oscillations, mixed-mode oscillations (subthreshold oscillations interspersed with spikes), clustering and bursting. In this manuscript we discuss biophysically plausible and phenomenological reduced models that preserve the biophysical and/or dynamic description of models of HH type and the ability to produce complex phenomena, but the number of effective dimensions (state variables) is lower. We describe several representative models. We also describe systematic and heuristic methods of deriving reduced models from models of HH type.

Abbreviations

FHN	FitzHugh–Nagumo (model)
HH	Hodgkin–Huxley (model)
HR	Hindmarsh–Rose (model)
ISI	Interspike interval
IF	Integrate-and-fire
LIF	Leaking integrate-and-fire (model)
ODE	Ordinary differential equation
PDE	Partial differential equation
STOs	Subthreshold oscillations
MMOs	Mixed-mode oscillations
1D, 2D, . . . ND	One-, two-, . . ., N-dimensional
I_L	Leak current
I_{Na}	Transient Na (spiking) current
I_{K}	Delayed rectifier K (spiking) current
I_{Nap}	Persistent Na current
I_{Ks}	Slow K current
I_{M}	M-type K current
I_{h}	Hyperpolarization-activated mixed Na/K current
I_{Ca}	(Persistent) Ca current
I_{CaT}	T-type Ca current
I_{CaL}	L-type Ca current
I_{AHP}	After-hyperpolarization current Ca-dependent K current
I_{AMP}	Persistent amplifying current
I_{RES}	Persistent resonant current
$I_{\mathrm{AMP/RES}}$	Transient amplifying/resonant current
I_X model	Model of HH type having one (X) current with two gating variables in addition to I_L
$I_X + I_Z$ model	Model of HH type having two (X and Z) currents with a single gating variable each in addition to I_L

Communicated by Benjamin Lindner.

✉ Horacio G. Rotstein
horacio@njit.edu

[1] Departamento de Matemática, Universidad Nacional del Sur and CONICET, Bahía Blanca, Argentina

[2] Courant Institute of Mathematical Sciences, New York University, New York, USA

[3] Federated Department of Biological Sciences, New Jersey Institute of Technology and Rutgers University, Newark, USA

Contents

Journal: 422 MS: 0960 ☐ TYPESET ☐ DISK ☐ LE ☐ CP Disp.:2023/3/25 Pages: 21 Layout: Large

1 Introduction

Mathematical and computational models of neuronal activity have played a significant role in the development of the field of neuroscience, particularly due to the complexity of the nervous system and the need to supplement the available experimental tools to interrogate neurons and neuronal circuits. Mathematical models have been used to understand the biophysical and dynamic mechanisms underlying neuronal function and the processing of neuronal information, to make predictions to be tested experimentally, and as constitutive components of hybrid experimental/computational tools (e.g., Prinz et al. 2004; Sharp et al. 1993a, b).

In this paper we focus on dynamic models of single neurons, assumed to be isopotential (point neurons), where the electric activity of the neurons is described by a relatively small system of ordinary differential equations (ODEs). We leave out the equally relevant statistical models of neuronal activity (Kass et al. 2018), the effects of stochastic components (e.g., intrinsic, synaptic and background noise) and the description of the spatial extension of neurons, all of which deserve separate papers.

We adopt the pragmatic view that models are constructed to understand certain phenomena with a variety of goals, and in the context of associated theories (see discussion in Levenstein et al. (2020) and references therein). As such, they can capture the phenomena at various, often qualitatively different and complementary levels of abstraction. Conductance-based models describe the electric circuit properties of neurons. Simulations of these models produce patterns of activity that can be fit to experimental results. In contrast, phenomenological models are constructed to reproduce certain observed patterns with no *a priori* link to the biophysical properties of neurons.

There is no well-defined notion of model low-dimensionality in the absence of a reference for model dimensionality (how many dimensions make a model low-dimensional?). Because models are dependent on the context and the phenomena that are investigated (experimental, computational or theoretical), we use a flexible notion of dimensionality reference based on the well-known (biophysical) conductance-based point-neuron Hodgkin–Huxley (HH) four-dimensional point neuron model (Hodgkin and Huxley 1952a, b) and its extensions to include additional ionic currents with the same conductance-based formalism, collectively referred to as models of HH type. Models are low-dimensional as compared to the dimensionality of a corresponding (reference) point-neuron model of HH type, provided they can be considered as "embedded" in or reduced versions of their reference model.

In Sect. 2 we describe the conductance-based models of HH type and discuss some of their properties that are relevant for the models discussed in the remainder of the paper. Low-dimensional models of HH type can be either systematically reduced from the reference models of HH type or constructed ad-hoc by using the same conductance-based formalism, but leaving out details that are not necessary for the description of the phenomenon to be investigated. We discuss these two approaches in Sects. 3 and 4. In Sect. 5 we discuss the construction of phenomenological (caricature) models. These models are not biophysically linked to the higher-dimensional models of HH type. Instead, phenomenological models are linked to the models of HH type

Journal: 422 MS: 0960 TYPESET DISK LE CP Disp.:2023/3/25 Pages: 21 Layout: Large

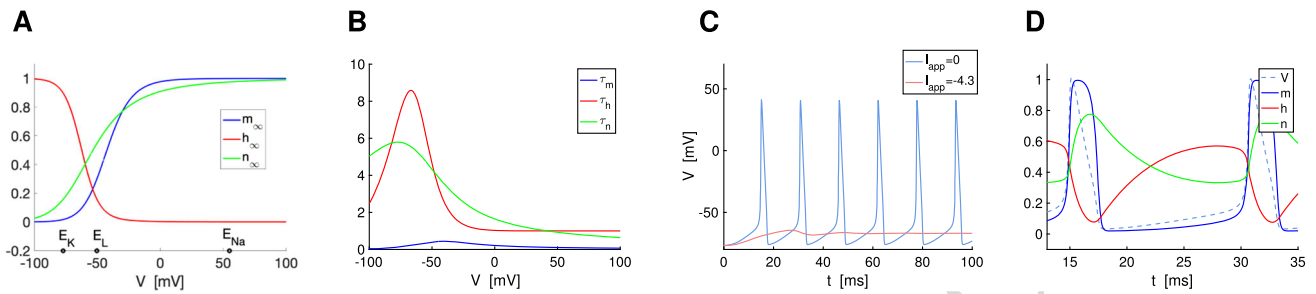

Fig. 1 The Hodgkin–Huxley model (1)–(2). **A** Voltage-dependent activation/inactivation curves. **B** Voltage-dependent time constants. **C** Representative examples of the time courses for V in the spiking ($I_{app} = 0$) and subthreshold oscillations ($I_{app} = -4.3$) regimes. **D** Representative example of the time courses for m, h and n during one spiking period (in between two action potentials) superimposed to the time course for V (adapted to fit in the range of the other variables) for $I_{app} = 0$. We used the parameter values adapted (Ermentrout and Terman 2010) from the original model (Hodgkin and Huxley 1952a)

by their phase-space descriptions; the phase-space diagrams of the phenomenological models can be considered as simplified versions of the phase-space diagrams of models of HH type. In Sect. 6 we discuss a number of methods to link phenomenological and biophysical models in order to make the former biophysically interpretable. In Sect. 7 we discuss the well-known leaky integrate-and-fire model (Abbott 1999; Brunel and van Rossum 2007; Hill 1936; Knight 1972; Lapicque 1907; Stein 1965, 1967) and a number of extensions collectively referred to as models of integrate-and-fire type. In addition to describing the models and how they are constructed, we discuss the different ways in which they can be made interpretable in terms of the biophysical properties of neurons. We present our final remarks in Sect. 8. A table of acronyms is presented at the end of the paper.

2 Conductance-based models of single neurons

2.1 The Hodgkin–Huxley (HH) model

Conductance-based models of single neurons describe the dynamics of the membrane potential (V) and a number of additional state variables associated to the participating ionic currents and other biophysical processes. Conductance-based models are constructed by first building an (equivalent) electric circuit representation (or model) of the neuronal circuit (e.g., Fig. 1 in Perkel et al. (1981) and Fig. 1 in Rotstein (2020)) and then writing the differential equations that mathematically describe the dynamics of these circuits in terms of the biophysical parameters. For point neurons, the models consist of nonlinear systems of ODEs.

The Hodgkin–Huxley (HH) model (Hodgkin and Huxley 1952a, b) is the prototypical conductance-based model that describes the generation of action potentials as the result of the interplay of the neuronal biophysical properties (Fig. 1). The spike generation mechanisms are explained in more detail in Sect. 2.4. In its simplest version, the neuron is assumed to be isopotential. The model describes the evolution of V (mV) and three dynamic variables associated to the transient sodium (I_{Na}) and delayed rectifier potassium (I_K) currents. The current-balance equation is given by

$$C\frac{dV}{dt} = -G_L(V - E_L) - G_{Na}m^3h(V - E_{Na}) - G_K n^4(V - E_K) + I_{app}, \quad (1)$$

where t is time (ms), C is the specific capacitance (μF/cm^2), G_Z ($Z = L, Na, K$) (μF/cm^2) are specific maximal conductances of the leak current I_L, I_{Na} and I_K, respectively, E_Z ($Z = L, Na, K$) (mV) are the corresponding reversal potentials, and I_{app} is the applied (DC) current (μA/cm^2).

The gating variables x ($= m, h, n$) obey differential equations of the form

$$\frac{dx}{dt} = \phi_x \frac{x_\infty(V) - x}{\tau_x(V)} \quad (2)$$

where $x_\infty(V)$ are voltage-dependent activation/inactivation curves (Fig. 1-A), $\tau_x(V)$ are voltage-dependent time constants (Fig. 1-B) and ϕ_x is a temperature coefficient (not present in the original HH model). The gating variables x decay towards the voltage-dependent functions $x_\infty(V)$ with a speed determined by the voltage-dependent time constants $\tau_x(V)$. Figure 1 shows representative examples of the time courses for V (Fig. 1-C) and the gating variables (Fig. 1-D).

2.2 The HH formalism: models of HH type

Strictly speaking, the HH model is the model described by Hodgkin and Huxley for the squid giant axon in their original paper (Hodgkin and Huxley 1952a). Over the years, the equations defining the HH model have been used with parameters fit to data other than the squid axon, giving rise to different models described by the same type of equations.

Journal: 422 MS: 0960 TYPESET DISK LE CP Disp.:2023/3/25 Pages: 21 Layout: Large

Moreover, the HH model has been extended by including additional terms describing a number (N_{ion}) of voltage- and concentration-gated ionic currents (e.g., Na^+ I_{Nap}, T-, L-, N-, P- and R-type Ca^{2+}, M-, A- and inward rectifying K^+, hyperpolarization-activated mixed Na^+/K^+ or h-, Ca^{2+}-activated K^+) to the current-balance equation, and additional equations describing the dynamics of the corresponding gating and concentration variables. We refer the reader to Ermentrout and Terman (2010) for a description of these currents.

The general form of the current-balance equation for models of HH type reads

$$C\frac{dV}{dt} = -I_L - \sum_{j}^{N_{\text{ion}}} I_{\text{ion,j}} + I_{\text{app}}. \tag{3}$$

The leak current is given by $I_L = G_L(V - E_L)$. The generic ionic currents $I_{\text{ion,j}}$ ($j = 1, 2, \ldots, N_{\text{ion}}$) can be either transient $I_X = G_X m^a h^b (V - E_X)$, having two gating variables (m,h), or persistent $I_Z = G_Z n^c (V - E_Z)$, having a single gating variable (n).

Spiking (non-reduced) models of HH type have the same or higher dimensions as compared to the classical HH model (but see Sects. 3 and 4) and can produce more complex behaviors, including bursting (Rinzel 1985a), mixed-mode oscillations (MMOs, subthreshold oscillations interspersed with spikes) (Brøns et al. 2008) and clustering (Fransén et al. 2004).

Models of HH type are extensively described in a number of textbooks (Borgers 2017; Dayan and Abbott 2001; Ermentrout and Terman 2010; Gabbiani and Cox 2017; Gerstner et al. 2014; Gerstner and Kistler 2002; Johnston and Wu 1995; Izhikevich 2006; Koch 1999; Miller 2018; Tuckwell 1988). We refer the reader there for additional details.

2.3 Systematic reduction of spatial dimensions: from multicompartmental to point neurons models

The HH model used in Hodgkin and Huxley (1952a) to investigate the propagation of action potentials along the squid giant axon is a partial differential equation (PDE). It extends the HH model to include a term involving the second derivative of V with respect to a space variable along the main axonal axis, assumed to be cylindrical. The resulting cable equation models are infinite-dimensional. More realistic models include a larger number of dendrites, dendritic branching and non-uniform geometric and electric properties along dendrites and across the dendritic tree, thus increasing the model complexity (Dayan and Abbott 2001).

Mathematical discretization of PDE neuronal models reduces the dimensionality to a finite number. However, this number is extremely large given the small size requirement for the mathematical approximation to hold.

The point neuron approximation described above, on the other extreme, assumes isopotentiality and drastically reduces the number of dimensions of the HH model to four (V, m, h, n). The number of dimensions of point neuron models of HH type depends on the number and nature of the participating currents. Point neurons are the minimal models that preserve the electric properties provided by these currents.

The multi-compartment approach (Dayan and Abbott 2001; Ermentrout and Terman 2010) is a compromise solution consisting of dividing the dendritic tree into a number of isopotential compartments. Multi-compartmental models preserve the spatial geometry of dendrites and dendritic trees as well as the nonuniformity of ionic currents distribution, while significantly reducing the model dimensionality by relaxing the requirement of being a mathematical approximation of PDE models. These models can be used to investigate the differential effects of dendritic vs. somatic inputs, which cannot be done with point neuron models.

Spatially extended models either PDE-based or multi-compartment models are beyond the scope of this article and will not be discussed further.

2.4 Generation of action potentials by the HH model

For low enough values of I_{app} in the HH model, V displays subthreshold oscillations (STOs, Fig. 1-C, light coral). For higher values of I_{app}, there is an abrupt transition to spikes (Fig. 1-C, light blue). The spiking dynamics result from the combined activity of the participating ionic currents and the associated positive and negative feedback effects provided by the participating gating variables.

From Fig. 1-A, the gating variables m and n activate by depolarization (activating variables), while the variable h activates by hyperpolarization (inactivating variable). As V increases, m and n increase and h decreases, but m evolves faster than h and n (Fig. 1-D), which are comparable. This is because the time constant for m is much smaller than the time constants for h and n (Fig. 1-B), and the membrane time constant $\tau = C/Gl \sim 3.33$. As a result, as V increases, first $I_{\text{Na}} = G_{\text{Na}} m^3 h(V - E_{\text{Na}})$ causes V to increase further (I_{Na} drives V towards the depolarized value of E_{Na}). This positive feedback effect gives rise to the rapid increase in V characterizing a spike. The negative feedback effects exerted by the delayed decrease of h and increase of n cause the spike to be terminated and a subsequent hyperpolarization ($I_{\text{K}} = G_K n^4 (V - E_K)$ drives V towards the hyperpolarized values of E_K). As V decreases, m and n decrease and h increases, allowing V to increase again (repolarize), thus initiating a new spiking cycle.

Journal: 422 MS: 0960 TYPESET DISK LE CP Disp.:2023/3/25 Pages: 21 Layout: Large

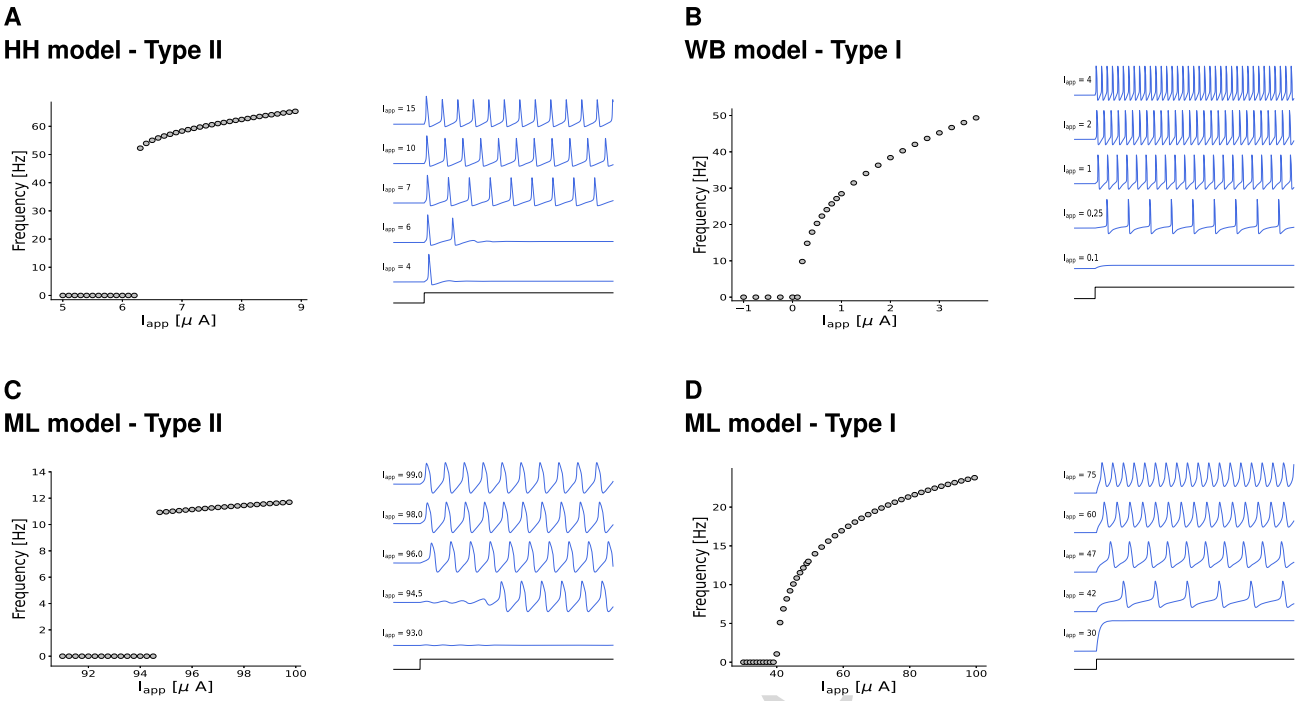

Fig. 2 Models of HH type: representative V **time courses and excitability types. A** Hodgkin–Huxley (HH) model (type II). The parameter values were taken from Ermentrout and Terman (2010) (Section 1.9). **B** Wang–Buzsaki (WB) model (type I). The parameter values were taken from Wang and Buzsáki (1996), $\phi = 0.5$. **C** Morris–Lecar (ML) model (type II). The parameter values were taken from Ermentrout and Terman (2010) (Section 3.1, second column in table 3.1). **D** Morris–Lecar (ML) model (type I). The parameter values were taken from Ermentrout and Terman (2010) (Section 3.1, third column in table 3.1)

2.5 Dynamical mechanisms of action potential generation: types I, II and III excitability

This excitability classification refers to the qualitatively different ways in which a neuron's activity transitions from rest to spiking as measured by the I_{app} versus spiking frequency (I–F) curves (Prescott et al. 2008a; Rinzel and Ermentrout 1998). Type I neurons admit arbitrarily small frequencies and therefore the I–F curves are continuous (Fig. 2-B, -D), while type II neurons have discontinuous I–F curves (Figs. 2-A and -C). Type II neurons, but not type I neurons, exhibit STOs when appropriately stimulated. The HH model (Hodgkin and Huxley 1952a) is type II (Fig. 2-A). An example of type I models is the Wang-Buzsaki model (Wang and Buzsáki 1996) (Fig. 2-B). The mechanisms underlying the two types of excitability (Fig. 2-C, -D) have been linked to different bifurcation scenarios (e.g., saddle-node on an invariant circle for type I and subcritical Hopf for type II) (Izhikevich 2006; Rinzel and Ermentrout 1998). We refer the reader to the detailed analysis presented in Izhikevich (2006). Type III neurons produce transient spikes in response to stimulation, instead of periodic (or repetitive) spiking (Meng et al. 2012; Prescott et al. 2008a). In this case, the I–F curve is undefined. We note that models of HH type having the same ionic currents may have different excitability mechanisms (Ermentrout and Terman 2010) when the currents operate in different parameter regimes. In other words, the type of ionic currents present in a model, per se, do not define the excitability mechanism.

The differences in the excitability mechanisms can be thought of as a characterization of the dynamics of single neurons, but they are also translated to differences in the responses of neurons to synaptic inputs as measured by the phase-response curves (PRCs) and the synchronization properties of the networks in which they are embedded (Ermentrout 1996; Ermentrout and Terman 2010; Hansel et al. 1995).

2.6 Integrators and resonators

This classification refers to the qualitatively different ways in which neurons summate inputs. Integrators do it across a wide range of frequencies, while resonators respond better to some (preferred) input frequencies and therefore respond more selectively to synchronized inputs (coincidence detectors). One classification is based on the existence (resonators) or absence (integrators) of intrinsic STO (typically damped) (e.g., Izhikevich 2006; Brette and Gerstner 2005). In the presence of oscillations, two inputs are more efficiently communicated upstream when they are separated by an interval

Journal: 422 MS: 0960 TYPESET DISK LE CP Disp.:2023/3/25 Pages: 21 Layout: Large

equal to the oscillation frequency than by other interval sizes. However, systems that do not exhibit STOs (sustained or damped) may exhibit subthreshold resonance (peak in the impedance amplitude profile in response to oscillatory inputs at a preferred, resonant, frequency) (Richardson et al. 2003; Rotstein and Nadim 2014) and may show sustained STOs in response to noise (e.g, Pena and Rotstein 2022). Integrators and resonators have been associated to type I and II excitability, respectively (e.g., Prescott et al. 2008b and references therein).

3 Systematic reduction of (state) dimensions of models of HH type

This process consists of reducing the number of state variables in the model without losing its ability to produce the same behavior to an acceptable level of approximation. The reduction process must preserve the type of excitability and the summation properties described above. We explain the main ideas for the HH model and briefly discuss extensions to other models of HH type.

3.1 Steady-state approximation of fast gating variables

When τ_m is much smaller than τ_h, τ_n (Fig. 1-B) and the membrane time constant τ, we can make the steady-state approximation $m = m_\infty(V)$ in Eq. (1) thus reducing the HH model dimensionality from four to three.

Remark The steady-state approximation can be applied to other variables with fast dynamics such as I_{Nap} activation (Butera et al. 1999). However, a more detailed analysis is required when multiple variables are candidates for the steady-state approximation and the small time constants are not comparable.

3.2 Unsuccessful elimination of dynamically redundant gating variables

The remaining two variables (h and n) are necessary for the HH model to produce action potentials and are biophysically different, but dynamically redundant in the sense that both provide negative feedback effects; both are resonant gating variables (their linearized conductances are positive) (Richardson et al. 2003; Rotstein and Nadim 2014) since h is depolarization-inactivated and is part of a depolarizing current and n is depolarization-activated but is part of a hyperpolarizing current. Disrupting either process by making either $h = 1$ or eliminating I_{K} from Eq. (1) reduces the model dimensionality to two. However, it causes a transition from (stable) limit cycle to (stable) fixed-point behaviors in the resulting 2D $I_{\text{Na}} + I_{\text{K}}$ and I_{Na} models (Fig. 6-C for $h = 1$ and Fig. 6-D for $G_K = 0$). Therefore, the reduced equations are not a "good" reduced model. The same occurs if one uses other constant values of h or n in Eq. (1).

Remark One can find 2D I_{Na} and $I_{\text{Na}} + I_{\text{K}}$ models (using $n = 0$ and $h = 1$, respectively) exhibiting (stable) limit cycle behavior that are formally a reduced version of 4D models of HH type, but for parameters different from the original models used (e.g., Izhikevich 2006). In general these reduced 2D models are not an approximation of the 4D models they are embedded in.

3.3 Successful resolution of the dynamic redundancy

An alternative, successful approach, pioneered in Rinzel (1985b), is based on the observation that h and n evolve in a quasi-symmetric manner with respect to a horizontal axis (Fig. 6-D) since their time constants are comparable in magnitude. Therefore, one can approximate one as a linear function of the other, thus reducing the model dimensionality to two and conserving the spiking limit cycle behavior (Fig. 6-A) with approximate attributes (e.g., spike frequency and amplitude). The resulting 2D model produces an approximate solution to the original (4D) HH model. The same type of approximations have been done in other models of HH type (Butera et al. 1999; Ermentrout and Kopell 1998). More details on the systematic approach and generalizations are provided in Rinzel (1985b), Gerstner et al. (2014), Kepler et al. (1990).

Remark The approach described here can be in principle used for other variables such as I_{Nap} inactivation and I_{Ks} activation when their time constants are comparable as in the models described in Butera et al. (1999).

3.4 Constant approximations of slow variables

This type of approximation can be used for the model's slowest variable (or variables if the slow time constants are comparable) provided the dynamics is slow enough as compared to the time scale of the dynamic behavior one wishes to reproduce (e.g., spiking period). However, eliminating a slow variable can qualitatively change the model's behavior, particularly in 3D models exhibiting MMOs and bursting, which are absent in 2D models (Butera et al. 1999; Rotstein et al. 2006).

Journal: 422 MS: 0960 TYPESET DISK LE CP Disp.:2023/3/25 Pages: 21 Layout: Large

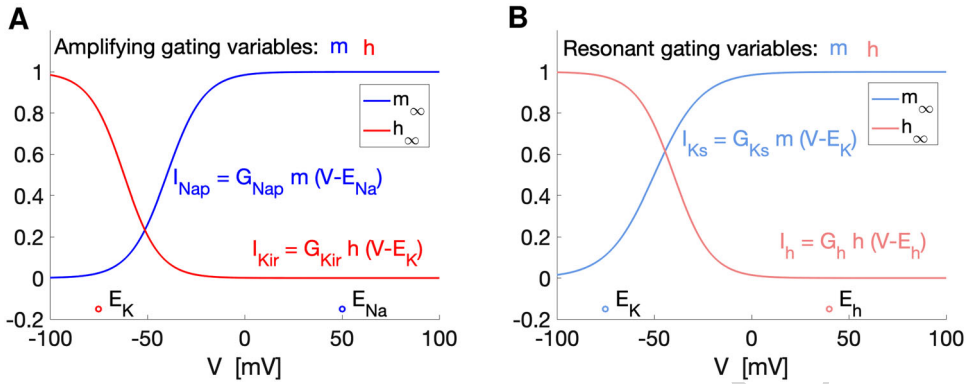

Fig. 3 Resonant and amplifying gating variables: representative examples. **A** Amplifying gating variables: (i) depolarization-activated for a depolarizing (inward) current (blue) or (ii) hyperpolarization-activated for a hyperpolarizing (outward) current (red). Examples are (i) persistent Na I_{Nap} and (ii) inward-rectifying potassium I_{Kir}. **B** Resonant gating variables: (i) depolarization-activated for a hyperpolarizing (outward) current (light blue) or (ii) hyperpolarization-activated for a depolarizing (inward) current (light coral). Examples are (i) slow K current I_{Ks} and (ii) hyperpolarization-activated mixed Na/K I_h. Currents having a single gating variable inherit the resonance/amplifying classification from their gating variables (e.g., I_{Nap}/ I_{Kir} are amplifying and I_h / I_{Ks} are resonant). Current having two gating variables (e.g., transient Na, T-type Ca) cannot be classified as resonant/amplifying. However, they have been classified as both in some cases (Hutcheon and Yarom 2000)

4 Construction of "reduced", biophysically plausible models of HH type

The models we describe here consist of a combination of ionic currents that do not generally include the spiking currents I_{Na} and I_{K}. They are able to produce primarily activity at the subthreshold level that control the resulting spiking patterns such as spike-frequency adaptation, and exhibit behaviors such as oscillations and resonance, but their dimensionality is low as compared to the spiking models of HH type in which they could be embedded (obtained by adding the spiking currents I_{Na} and I_{K}).

While in the absence of these currents the models do not describe the spiking dynamics, for certain parameter regimes they describe the onset of spikes (Izhikevich 2006; Rotstein et al. 2006; Rotstein 2017a), and can be supplemented with a mechanism of spike detection or spike generation (if the onset of spikes is not described by the model) and reset values for the participating variables, thus generating "artificially" spiking models of integrate-and-fire (IF) type.

What differentiates the modeling approaches described here and in Sect. 3 is the perspective. The models described here are constructed ad-hoc. They are not formally reduced from higher-dimensional spiking models as we did in Sect. 3, but they can be embedded in (higher-dimensional) spiking models. The two ("top-down" and "bottom-up") processes are not always reversible since the elimination of the spiking currents is expected to qualitatively affect the subthreshold dynamics (e.g., Jalics et al. 2010, compare with Rotstein et al. 2006).

In principle, any active current ($I_{\text{ion,j}}$) or combination of currents in Eq. (3) produces a model. However, models are constructed with a purpose. Therefore, here we only describe a number of representative models and general principles to construct them, which can be applied to specific situations. The simplest possible conductance-based model is for a passive cell having no active currents

$$C\frac{\mathrm{d}V}{\mathrm{d}t} = -G_L\,(V - E_L) + I_{\text{app}} \tag{4}$$

Next in line of complexity are 1D nonlinear models. By necessity, these models have instantaneously fast ionic currents added to Eq. (4). Their presence generates nonlinearities in the otherwise linear passive cell model giving rise to phenomena such as bistability, and the associated voltage threshold, in certain parameter regimes (Izhikevich 2006).

4.1 Resonant and amplifying gating variables

This classification is based on the dynamic properties of the gating variables, as defined by the kinetic equation (2), and the properties of the ionic currents in which they are embedded (see Sect. 2.2) (Izhikevich 2006; Richardson et al. 2003; Rotstein and Nadim 2014).

Resonant gating variables can be either hyperpolarization-activated within an outward current (Fig. 3-B, light coral) or depolarization-activated within an inward current (Fig. 3-B, light blue). They provide a negative feedback effect endowing the ability of the models to produce resonance and oscillations. Amplifying gating variables, in contrast, can be either depolarization-activated within an inward current (Fig. 3-A, blue) or hyperpolarization -activated within an outward current (Fig. 3-A, red). They provide a positive feedback effect enhancing the voltage responses to external

Journal: 422 MS: 0960 TYPESET DISK LE CP Disp.:2023/3/25 Pages: 21 Layout: Large

inputs and creating sustained oscillations. We use the notation I_{RES} and I_{AMP} for persistent ionic currents having a single resonant or amplifying gating variables, respectively, and $I_{RES/AMP}$ for transient ionic currents having both a resonant and an amplifying gating variables. We refer to the persistent currents having instantaneously fast gating variables as instantaneously fast currents.

4.2 I_{AMP} + I_{RES} 2D models

The I_{AMP} + I_{RES} models combine an instantaneously fast current I_{AMP} (e.g., I_{Nap}, I_{Kir}, I_{Ca}) and a slower current I_{RES} (e.g., I_{h}, I_{Ks} or I_{M}). The current-balance equation is given by

$$C\,\frac{\mathrm{d}V}{\mathrm{d}t} = I_{\mathrm{app}} - I_L - I_{\mathrm{AMP}}(V) - I_{\mathrm{RES}}(V,h) \tag{5}$$

where $I_{\mathrm{AMP}}(V) = G_X m_\infty^a(V)(V - E_X)$ and $I_{\mathrm{RES}}(V,n) =. G_Z n^c (V - E_Z)$. The gating variable n obeys an equation of the form (2).

Remark 1. Additional possible 2D models include: (i) I_{RES} and I_{AMP} models where the gating variables are not instantaneously fast, (ii) I_{AMP} + I_{AMP} models with an instantaneously fast and a slower gating variables, and (iii) I_{AMP} + I_{RES} models with more than one instantaneously fast amplifying gating variable.

Remark 2. The 2D I_{Na} + I_{K} reduced version of the HH model discussed in Sect. 3 (elimination of the dynamics for h) formally belongs to this category.

4.3 $I_{AMP/RES}$ 2D models

They have a single current $I_{\mathrm{AMP/RES}}$ combing an instantaneously fast amplifying gating variable (e.g., I_{Ca} activation, I_A activation) and a slower resonant gating variable (e.g., I_{Ca} inactivation, I_A inactivation). The current-balance equation is given by

$$C\,\frac{\mathrm{d}V}{\mathrm{d}t} = I_{\mathrm{app}} - I_L - I_{\mathrm{AMP/RES}}(V,h) \tag{6}$$

where $I_{\mathrm{AMP/RES}}(V,h) = G_X m_\infty^a(V) h^b (V - E_X)$. The gating variable h obeys an equation of the form (2). Prototypical examples models having a T-type Ca current (I_{CaT}) and the A-type K current (I_A) (Golomb et al. 2006; Manor et al. 1997; Torben-Nielsen et al. 2012; Wang and Rinzel 1992).

Remark 1. Additional 2D models include I_{AMP} + $I_{\mathrm{AMP/RES}}$ (2D) models with two instantaneously fast amplifying gating variables.

Remark 2. The 2D I_{Na} reduced version of the HH model discussed in Sect. 3 (elimination of I_{K}) formally belongs to this category.

4.4 The Morris–Lecar (ML) model (I_{Ca}+I_K)

The Morris–Lecar model belongs to the category described in Sect. 4.2 (with $I_{\mathrm{AMP}} = I_{\mathrm{Ca}}$ and $I_{\mathrm{RES}} = I_{\mathrm{K}}$), but it deserves a special mention given its historical importance.

The current balance equation for the 2D version (Rinzel and Ermentrout 1998) of the Morris–Lecar (ML) model (Morris and Lecar 1981) is given by

$$C\,\frac{\mathrm{d}V}{\mathrm{d}t} = I_{\mathrm{app}} - I_L - I_{\mathrm{Ca}}(V) - I_{\mathrm{K}}(V,w) \tag{7}$$

where $I_{\mathrm{Ca}}(V) = G_{\mathrm{Ca}}\, m_\infty(V)\,(V - E_{\mathrm{Ca}})$ and $I_{\mathrm{K}}(V,w) = G_K\, w\,(V - E_K)$. The gating variable w obeys an equation of the form (2). Examples of dynamics of the ML model are shown in Fig. 2-C and -D. A more detailed description of the model as well as parameter regimes where the model exhibits type I and type II excitability and different type of dynamical systems bifurcations can be found in Ermentrout and Terman (2010) (see also Lecar 2007).

4.5 I_{AMP} + I_{RES} and $I_{AMP/RES}$ 3D models

These models include the models described above where the two gating variables are non-instantaneous. They also include models having one instantaneously fast amplifying gating variable and two slower resonant gating variables such as a two-component h-current or a combination of h- and M-currents (Acker et al. 2003; Rotstein et al. 2006; Richardson et al. 2003; Rotstein 2017a). This type of models can produce phenomena such subthreshold resonance and antiresonance (Richardson et al. 2003; Rotstein 2017a) (a peak followed by a trough in the impedance amplitude profile) and MMOs when they are embedded in higher-dimensional models of HH type having I_{Na} and I_{K} or models of integrate-and-fire type (described below). MMOs are inherently 3D (or higher-dimensional) phenomena. 2D I_{AMP} + I_{RES} and $I_{\mathrm{AMP/RES}}$ models can produce either STOs or the onset of spikes, but not both. The coexistence of STOs and the onset of spikes requires 3D or higher-dimensional models. Action potential clustering (Fransén et al. 2004), a type of irregular MMO pattern (e.g., Fig. 8 in Fransén et al. 2004) can occur in the presence of additional currents or noise.

4.6 Bursting models (3D and 4D)

Bursting patterns, consist of barrages of spikes separated by quiescent intervals of time, which are longer than the interspike interval (ISI) (Rinzel 1986; Coombes and Bressloff 1999; Bertram et al. 1995). Bursting patterns are also inherently 3D (or higher-dimensional) phenomena since, roughly speaking, they consist of two intertwined processes (fast oscillations and burst envelope dynamics, alternating

Journal: 422 MS: 0960 TYPESET DISK LE CP Disp.:2023/3/25 Pages: 21 Layout: Large

between an active and quiescent phases), each of which requires at least 2D dynamics. To some extent the minimal models of bursting belong to the category discussed in this section. However the number of types of bursting patterns and models that can generate them are very large. We refer the reader to Coombes and Bressloff (1999), Izhikevich (2006) for detailed discussions on models of bursting.

5 Phenomenological (caricature) models: geometric/phase-plane simplification of models of HH type

Phenomenological models of neuronal dynamics capture patterns of activity and dynamic phenomena observed in neuronal and excitable systems (e.g., the existence of a resting potential and a voltage threshold for spike oscillations, neuronal relaxation oscillations, spiking activity, bursting activity, clustering, MMOs, and depolarization block), but their constitutive equations are not constructed from biophysical laws or processes (e.g., current-balance by Ohm's law, kinetics of opening and closing of ion channels). Instead, the phenomenological equations are simpler and motivated by the phenomena that emerge from these processes.

The type of phenomenological models we discuss here are linked to the models of HH type by the geometric structure of the phase-plane diagrams. Specifically, the zero-level sets in the phase-plane diagrams (e.g., nullclines in 2D models and nullsurfaces in 3D models) are simplified versions of their counterparts in the models of HH type (e.g., cubic-like and sigmoid nullclines become cubics and lines; compare Fig. 6-A_2 and -B_2). For a discussion on the emergence of cubic nonlinearities in neuronal models as the result of the presence of regenerative (amplifying) currents we refer the reader to Izhikevich (2006), Rotstein (2017b). In this sense, they are phase-plane simplifications of models of HH type.

5.1 Models of FitzHugh–Nagumo (FHN) type

The general form of the models of FitzHugh–Nagumo (FHN) type is given by

$$\frac{dV}{dt} = -h\,V^3 + a\,V^2 - w, \tag{8}$$

$$\frac{dw}{dt} = \epsilon\,[\alpha\,V - \lambda - w\,], \tag{9}$$

where h, a, ϵ, α and λ are constants, assumed to be positive with the exception of λ that can assume any real value. The (activator) variable V represents the membrane potential and the (inhibitor) variable w represents the recovery variable (n in the HH model). The parameter λ is interpreted as $I_{\rm app}$ in models of HH type; by a linear transformation ($w \to w + \lambda$) λ can be moved to the first equation. The parameters a and h control the shape of the V-nullcline ($w = -h\,V^3 + a\,V^2$). The local minimum of the V-nullcline occurs at $(0, 0)$. The maximum of the V-nullcline occurs at $(2/3\,a\,h^{-1}, 4/27\,a^3\,h^{-2})$, which is equal to $(1, 1)$ for the canonical parameter values $h = 2$ and $a = 3$. The parameters α and λ control the slope of the w-nullcline ($w = \alpha\,V - \lambda$) and its displacement with respect to the V-nullcline, respectively. The parameter ϵ represents the time-scale separation between the variables V and w.

The FHN model is a phase-plane simplification of 2D models of HH-type where the cubic-like V- and sigmoid-like w-nullclines in the reduced (2D) HH model (Fig. 6-A_2) become a purely cubic and linear, respectively (Fig. 6-B_2).

In addition to the neuronal phenomena mentioned above (except for bursting, clustering and mixed-mode oscillations that required at least 3D models), models of FHN type exhibit the two types of Hopf bifurcations (sub- and super-critical) underlying neuronal excitability. The form of the model equations is different (e.g., $h = -1/3$ and $a = 1$), but the geometry of the phase-plane diagram is the same.

The original FHN model or Bonhoeffer van der Pol (BVP) model (Bonhoeffer 1948; FitzHugh 1961, 1960; Nagumo et al. 1962) was developed as an extension of the van der Pol (VDP) model for relaxation oscillations in electrical circuits (van der Pol 1920).

5.2 Extended and modified models of FHN type

5.2.1 Sigmoid recovery variable and voltage-dependent time scale separation

Additional flexibility can be obtained in shaping the oscillatory patterns in models of FHN type by substituting the linear w-nullcline by a sigmoid function and making the parameter ϵ dependent on V.

$$\frac{dV}{dt} = -h\,V^3 + a\,V^2 - w, \tag{10}$$

$$\frac{dw}{dt} = \epsilon(V)\,[\,G(\alpha V - \lambda) - w\,], \tag{11}$$

where $G(V) = G_{\rm amp}[1 + \exp(-V)]^{-1} - G_m$, and $G_{\rm amp}$ and G_m are non-negative constants.

5.2.2 Piecewise-linear cubic-like and sigmoid-like nullclines (nullsurfaces)

In order to make models of FHN type more amenable to mathematical analysis beyond the qualitative analysis using the phase-plane diagram, one can simplify them by substituting the cubic function $-hV^3 + aV^2$ in Eq. (8) by a cubic-like piecewise-linear (PWL) function (Rotstein et al. 2012) (and

Journal: 422 MS: 0960 ☐ TYPESET ☐ DISK ☐ LE ☐ CP Disp.:2023/3/25 Pages: 21 Layout: Large

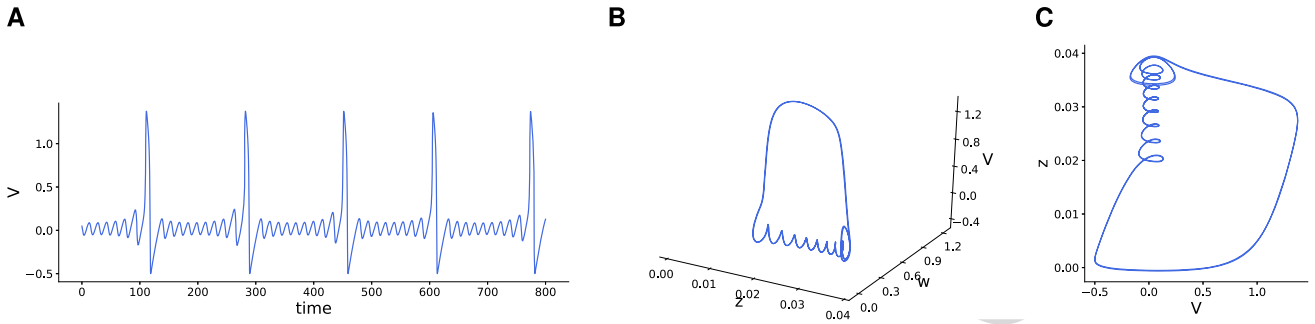

Fig. 4 Mixed-mode oscillations (MMOs) in the 3D model of FitzHugh–Nagumo (FHN) type: representative example. **A** V-time course. The small amplitude (subthreshold) oscillations are interspersed with large amplitude oscillations (spikes). **B** Limit cycle trajectory in the (3D) phase-space. **C** Projection of the limit cycle trajectory on the V-Z plane. We used Eqs. (12)–(14) with the following parameter values: $h = 2$, $a = 3$, $\epsilon = 0.1$, $\alpha = 2$, $\eta = 0.045$, $\beta = -1$ and $\sigma = -0.085$

references therein). The model can be further modified to have a sigmoid-like PWL w-nullcline.

5.2.3 3D model of FHN type

The 2D models of FHN type can exhibit fixed-points, subthreshold (small amplitude) oscillations, large amplitude oscillations (e.g., spikes) and ("static") transitions between sub- and supra-threshold phenomena as a parameter (e.g., λ) changes and the system undergoes a Hopf bifurcation. For small enough values of ϵ (time scale separation), these transitions are abrupt; the system exhibits the canard phenomenon (Krupa and Szmolyan 2001). The addition of a third equation (state dimension) endows the models with the ability to produce MMOs (Brøns et al. 2008; Rotstein et al. 2008; Golomb 2014) by dynamic transitions between sub- and supra-threshold behavior via a slow-passage through a Hopf bifurcation (Baer et al. 1989) and the 3D canard phenomenon (Szmolyan and Wechselberger 2001; Wechselberger 2005). The 3D models of FHN type read

$$\frac{dV}{dt} = -h\,V^3 + a\,V^2 - w, \tag{12}$$

$$\frac{dw}{dt} = \epsilon\,[\alpha\,V - z - w\,], \tag{13}$$

$$\frac{dz}{dt} = \epsilon\,\eta\,[\beta\,V - \sigma - z\,], \tag{14}$$

where σ is a parameter (similarly to λ in the 2D models of FHN type, σ captures the effect of constant inputs to the equation for V) and the parameter η represents the time scale separation between the variables w and z.

Several authors have used a simpler 3D model of FHN type where the right-hand side of Eq. (14) is substituted by $\epsilon\eta$ (erasing the square brackets). These models can display canard-based MMOs (Fig. 4) and the classical slow-passage through a Hopf bifurcation (Baer et al. 1989) in addition to regular oscillations and other types of patterns.

5.3 Hindmarsh–Rose (HR) model

The HR model is a 3D phenomenological (caricature) model designed to investigate the bursting behavior in neuronal models (Fig. 5). Two variables (V and y, or w) are responsible for the generation of spikes, while the third variable (z, or u) captures the effect of an adaptation current, which is responsible for creating and controlling the interspike-burst intervals.

The general form of the HR model (Hindmarsh and Rose 1994) is

$$\frac{dV}{dt} = -hV^3 + aV^2 + y - z + I_{\text{app}}, \tag{15}$$

$$\frac{dy}{dt} = c - \gamma V^2 - y, \tag{16}$$

$$\frac{dz}{dt} = r\,[\,\alpha(V - V_r) - z\,], \tag{17}$$

where h, a, I_{app}, c, γ, r, α and V_r are parameters.

A change of variables $w = -y + z - I_{\text{app}}$, $u = z(r-1) + c + I + r\alpha V_r$ brings the system (15)–(17) to

$$\frac{dV}{dt} = -hV^3 + aV^2 - w, \tag{18}$$

$$\frac{dw}{dt} = \gamma V^2 + \eta V - w - u, \tag{19}$$

$$\frac{du}{dt} = \frac{\eta}{\alpha}\,[\,(\eta - \alpha)V + \lambda - u\,] \tag{20}$$

where $\lambda = c + I_{\text{app}} + sV_r$ and $\eta = r\,s$, and reduces the number of parameters. This modified HR models has a form reminiscent to the FHN model described above. Note that as for the FHN model, the effect of the applied current I_{app} is included in the parameter λ. If $\eta = 0$, then $u = \lambda - \alpha V$ and $dw/dt = \gamma V^2 + \alpha V - \lambda - w$. If, in addition, $\gamma = 0$, the HR model reduces to the FHN model with $\epsilon = 1$.

Journal: 422 MS: 0960 TYPESET DISK LE CP Disp.:2023/3/25 Pages: 21 Layout: Large

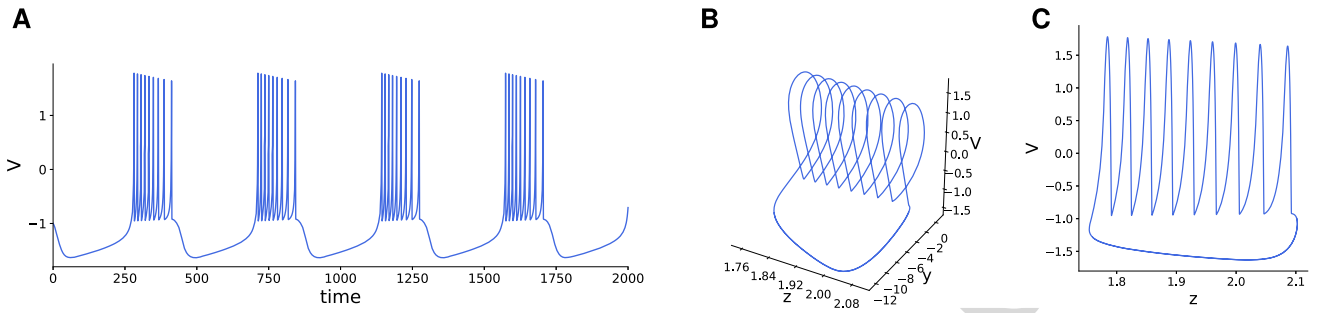

Fig. 5 Bursting in the Hindmarsh-Rose (HF) model: representative example. **A** V-time course. **B** Limit cycle trajectory in the (3D) phase-space. **C** Projection of the limit cycle trajectory on the V-Z space. We used Eqs. (15)–(17) with the following parameter values: $h = 1, a = 3, c = 1, \gamma = 5, r = 0.001, \alpha = 4, V_r = -1.6, I_{\text{app}} = 2$

5.4 Linear models

Linear models have been used to investigate the subthreshold dynamic properties of neurons and as the subthreshold component (substrate) of artificially spiking models of integrate-and-fire type (described later in the paper) (Izhikevich 2001; Rotstein 2013). The general form of the 2D linear models is

$$\frac{dV}{dt} = aV - bw, \tag{21}$$

$$\frac{dw}{dt} = cV - dw. \tag{22}$$

The parameter values are assumed to be either dimensionless or dimensional, but not linked to the biophysical properties of the neuron. This model can be further reduced to a model with two dimensionless parameters. When $b = c = d = 0$, Eq. (21) is a rescaled version of the passive membrane equation. When $d = a$ and $b = c$, Eqs. (21)–(22) are the subthreshold component of the so-called resonate-and-fire model (Izhikevich 2001).

5.5 Models of quadratic type

These models and variations have been developed to investigate the subthreshold nonlinear dynamic properties of neurons and as the subthreshold component of the quadratic integrate-and-fire model (1D subthreshold dynamics) (Ermentrout 1996) (see also Latham et al. 2000; Hansel and Mato 2001; Ermentrout and Kopell 1986) and its extension (2D subthreshold dynamics), the so-called Izhikevich model (Izhikevich 2010, 2003, 2006)

$$\frac{dV}{dt} = V^2 - w + I, \tag{23}$$

$$\frac{dw}{dt} = a(bV - w). \tag{24}$$

The right-hand sides of the equation for V in Izhikevich (2003) reads $0.04V^2 + 5V - w + I$. The right-hand sides of eqs. for V and w in Izhikevich (2010) read $k(V - V_{\text{rest}})(V - V_{\text{threshold}}) - w + I$ (divided by C) and $a[b(V - V_{\text{rest}}) - w]$, respectively.

The model parameters are phenomenologically linked to the neuronal properties, but they are not interpretable in terms of the biophysical properties of neurons.

6 Linking phenomenological and biophysical models: linearization and quadratization of models of HH type

The linearization (Richardson et al. 2003; Rotstein and Nadim 2014) and quadratization (Rotstein 2015; Turnquist and Rotstein 2018) processes described below provide ways to link linear and quadratic models, respectively, to the more realistic models of HH type and thus provide a biophysical interpretation to the model parameters and the results using these reduced models. The linearization process capitalizes on Taylor expansions around the fixed-point (up to the first order). The quadratization process consists of systematically fitting a quadratic function to the V-nullcline of a model of HH type. It also involves Taylor expansions (up to the second order), but instead of calculating this Taylor expansion around the fixed point, they are calculated around the local minimum/maximum of the V nullcline. In both cases, the process can be extended to arbitrary orders of the Taylor expansion. We describe in detail both processes for 2D models. It can be generalized to include additional gating variables (Richardson et al. 2003; Rotstein 2017a; Turnquist and Rotstein 2018).

6.1 Linear models and linearization of models of HH type

Linearization consists on expanding the right-side of the model differential equations into Taylor series around the relevant fixed-point and neglecting all the terms with power bigger than one.

Journal: 422 MS: 0960 TYPESET DISK LE CP Disp.:2023/3/25 Pages: 21 Layout: Large

We described the process for a 2D model of HH type (3) with two ionic currents ($N_{\text{ion}} = 2$) where

$$I_{\text{ion,j}} = G_j x_j (V - E_j), \tag{25}$$

the dynamics of x_1 are governed by Eq. (2) and $x_2 = x_{2,\infty}(V)$. The extension to higher-dimensional models with additional ionic currents is straightforward (Richardson et al. 2003; Rotstein and Nadim 2014; Rotstein 2018, 2017a).

The linearized 2D model around the fixed-point $(\bar{V}, \bar{x}_1)$ is given by

$$C \frac{\mathrm{d}V}{\mathrm{d}t} = -g_L v - g_1 w_1, \tag{26}$$

$$\tau_1 \frac{\mathrm{d}w_1}{\mathrm{d}t} = v - w_1, \tag{27}$$

where

$$v = V - \bar{V} \qquad w_1 = \frac{x_1 - \bar{x}_1}{x'_{1,\infty}(\bar{V})}, \tag{28}$$

with $g_j = G_j\, x'_{j,\infty}(\bar{V})\, (\bar{V} - E_j)$ $(j = 1, 2)$ and $g_L = G_L + g_2 + G_1\, x_{1,\infty}(\bar{V}) + G_2\, x_{2,\infty}(\bar{V})$.

Figure 7-A$_2$ illustrates this for a I_h+I_{Nap} model (see Fig. 7-A$_1$). Figure 7-B illustrates that the phase-plane structure in Fig. 7-A$_1$ is representative of a larger class of models. Geometrically, the linearization process consists of substituting the nullclines by lines intersecting at the fixe-point and tangent to the corresponding nullclines. Note that the sign of the denominator in the second equation (28) is positive (negative) provided x_1 is activating (inactivating), and therefore the corresponding phase-plane diagrams are mirror images of each other. In other words, the linearization process inverts the phase-plane diagram of models with inactivating gating variables with respect to the V axis.

Linearized models can be supplemented with a threshold for spike generation (V_{thr}) and reset values for the participating variables leading to models of integrate-and-fire (IF) type. The leaky integrate-and-fire (LIF) (Lapicque 1907) and resonate-and-fire (Izhikevich 2001) models are particular cases of this formulation.

As an approximation to models of HH type, the validity of linearized models is limited. However, linear models can be used as neuronal models in their own right by implicitly assuming the underlying dynamics are quasi-linear or to test theoretical ideas.

6.1.1 Linearized 3D models

The linearization process described above can be naturally extended to higher dimensions (see Richardson et al. 2003; Rotstein 2017a for details) with two gating variables x_1 and x_2 with non-instantaneous dynamics and a third variable $x_3 = x_{3,\infty}(V)$. The linearized 3D equations consist of Eq. (26) with an additional term $-g_2 w_2$, Eq. (27) for the variable w_1, and an additional equation for variable w_2 similar to Eq. (27).

6.2 Models of quadratic type and quadratization of models of HH type

Quadratization extends the notion of linearization with some subtle modifications that improve the approximations (compare Figs. 7-A$_2$ and -A$_3$) and, most importantly, capture more realistic aspects of the dynamics of models of HH type. We describe the process for the 2D model used to describe the linearized models. An extension to 3D models of HH type is briefly discussed at the end of this section. A further extension including time-dependent current and synaptic inputs is presented in Turnquist and Rotstein (2018).

One important assumption is that the V-nullcline is parabolic-like in the subthreshold regime (Fig. 7-A$_1$ and -B). This is a rather general property of neuronal models of HH type having regenerative (amplifying) ionic currents (e.g., Fig. 6-A$_2$) (see also Izhikevich 2006; Rotstein 2017b, a).

The quadratization process (Rotstein 2015; Turnquist and Rotstein 2018) consists on expanding the right-side of the model differential equations into Taylor series around the minimum/maximum (V_e,$x_{1,e}$) of the parabolic-like V-nullcline in the subthreshold regime, neglecting all the terms with power bigger than two in the equation for V and bigger than one in the equation for x_1, and translating the minimum/maximum of the V-nullcline to the origin.

The quadratized 2D model around (V_e,$x_{1,e}$) is given by

$$\frac{\mathrm{d}V}{\mathrm{d}t} = \sigma a v^2 - w, \tag{29}$$

$$\frac{\mathrm{d}w}{\mathrm{d}t} = \epsilon\, [\, \alpha\, v - \lambda - w\,], \tag{30}$$

where

$$v = V - V_e - \frac{g_L}{2\,\sigma\, g_c}, \tag{31}$$

$$w = \frac{g_1}{C} \frac{x_1 - x_{1,e}}{x'_{1,\infty}(V_e)} - \frac{F_e}{C} + \frac{g_L^2}{4\,\sigma\, g_c\, C}, \tag{32}$$

$$g_L = G_L + G_1\, x_{1,e} + G_2\, x_{2,\infty}(V_e) + g_2, \tag{33}$$

$$g_j = G_j\, (V_e - E_j)\, x'_{j,\infty}(V_e), \qquad j = 1, 2 \tag{34}$$

$$\sigma\, g_c = -\frac{G_2\, x''_{2,\infty}(V_e)\, (V_e - E_2) + 2\, G_2\, x'_{2,\infty}(V_e)}{2}, \tag{35}$$

$$\epsilon = \frac{1}{\tau_1(V_e)}, \qquad a = \frac{g_c}{C}, \qquad \alpha = \frac{g_1\,(1-\xi)}{C}, \tag{36}$$

$$\lambda = \frac{F_e}{C} - \frac{g_L^2}{4\,\sigma\, g_c\, C} - \frac{g_1\, \beta}{C} - \frac{g_1\,(1-\xi)}{2\,\sigma\, g_c\, C}\, g_L, \tag{37}$$

Journal: 422 MS: 0960 ☐ TYPESET ☐ DISK ☐ LE ☐ CP Disp.:2023/3/25 Pages: 21 Layout: Large

$$\beta = \frac{x_{1,\infty}(V_e) - x_{1,e}}{x'_{1,\infty}(V_e)}, \qquad \xi = \beta\,\frac{\tau'_1(V_e)}{\tau_1(V_e)}, \tag{38}$$

and

$$F_e = F(V_e, x_{1,e}) = I_{\rm app} - G_L\,(V_e - E_L) \\ -G_1\,x_{1,e}\,(V_e - E_1) - G_2\,x_{2,\infty}(V_e)\,(V_e - E_2). \tag{39}$$

The parameter a is assumed to be positive. The product $\sigma\,a$ controls the curvature of the parabolic V-nullcline. The concavity sign is captured by $\sigma = \pm 1$. By an appropriate change of variables when $\sigma = -1$ (concave down parabolic v-nullcline) the model can be transformed into one having a concave up parabolic v-nullcline. The parameter ϵ represents the time scale separation between the participating variables.

Quadratized models can be supplemented with a threshold for spike generation and reset values for the participating variables leading to models of integrate-and-fire (IF) type with parabolic V-nullclines. The quadratic integrate-and-fire (QIF) model and the phenomenological model proposed in Izhikevich (2003, 2010) are particular cases of this formulation. Importantly, in contrast to the linear models of IF type where $V_{\rm thr}$ is the mechanisms for spike generation (hard $V_{\rm thr}$), for quadratic models, the mechanism for spike generation is embedded in the model and the role of $V_{\rm thr}$ is simply to indicate the occurrence of a spike (soft $V_{\rm thr}$).

With certain limitations (inherent to any approximation, see assumptions), quadratized models provide a rather good approximation to models of HH type in the subthreshold regime. In addition, models of quadratic type can be used as neuronal models on their own right by implicitly making the above assumptions or to test theoretical ideas.

Possible extensions include considering parabolic nonlinearities for the dynamics of the gating variables.

6.2.1 Quadratized 3D models

The quadratization process described above can be naturally extended to higher dimensions (see Turnquist and Rotstein 2018 for details) for models with two gating variables x_1 and x_2 with non-instantaneous dynamics and a third variable $x_3 = x_{3,\infty}(V)$.

The quadratized 3D model around $(V_e,x_{1,e})$ is given by

$$\frac{{\rm d}V}{{\rm d}t} = \sigma a v^2 - w, \tag{40}$$

$$\frac{{\rm d}w}{{\rm d}t} = \epsilon\,[\,\alpha\,v - z - w\,], \tag{41}$$

$$\frac{{\rm d}z}{{\rm d}t} = \epsilon\,\eta\,[\,-\gamma\,v - z + \lambda\,]. \tag{42}$$

The description of the process as well as the definition of the additional model parameters in terms of the biophysical parameters of the models of HH type are presented in Turnquist and Rotstein (2018).

7 Models of integrate-and-fire (IF) type

7.1 The leaky integrate-and-fire (LIF) model

The LIF model (Stein 1967; Abbott 1999; Brunel and van Rossum 2007; Hill 1936; Knight 1972; Lapicque 1907; Stein 1965) is an abstraction of a neuronal circuit consisting of the passive membrane equation (4), representing an RC electric circuit, supplemented with a V threshold for spike generation ($V_{\rm thr}$) and a V reset value after a spike has occurred (V_{rst}). The spike times (defined as the times at which V reaches $V_{\rm thr}$) can be recorded and spikes may be visualized with a vertical line at the spiking times (Fig. 8-A1). LIF models exhibit type I excitability (the frequency vs. applied current curve admits infinitely small frequencies as the applied current increases.).

The LIF model predates the HH model, but it can be thought of as a simplification of the HH model where the spiking currents ($I_{\rm Na}$ and $I_{\rm K}$) are eliminated, their effects at the subthreshold level are partially absorbed by I_L (by the process of linearization described in Sect. 6.1) and the spiking dynamics are substituted by the parameters $V_{\rm thr}$ and V_{rst}. LIF models may include additional parameters representing an explicit refractory period (T_{refr}) and a spike duration (T_{dur}, necessary for the development of some intrinsic and synaptic currents). Additional modifications of the LIF model (e.g., varying thresholds) and their functionality are discussed in Burkitt (2006), Fuortes and Mantegazzini (1962).

While the subthreshold dynamics are 1D, the LIF model is effectively higher-dimensional, but simpler than the models of HH type.

7.2 Construction of models of IF type

The LIF models (and modified/rescaled versions) have been extensively used Burkitt (2006) due to their relative simplicity and have led the way to a series of models designed to overcome their flaws (Brunel and van Rossum 2007; Izhikevich 2006). Common to all these, more complex models is an explicit description of the subthreshold dynamics in terms of differential equations (phenomenological models of models of HH type) and "artificial" spikes characterized by V_{trh}, V_{rst}, T_{refr}, T_{dur} and reset values for the additional subthreshold variables when necessary. These parameters need to be estimated from the observed patterns. In some models (e.g., LIF, see also Izhikevich 2001; Rotstein 2017a), $V_{\rm thr}$ determines the mechanism of spike generation (hard threshold). In others, the subthreshold dynamics describe the onset of spikes (V diverges to infinity in finite time, interpreted as the variables "escaping" the subthreshold regime and activating

Journal: 422 MS: 0960 ☐ TYPESET ☐ DISK ☐ LE ☐ CP Disp.:2023/3/25 Pages: 21 Layout: Large

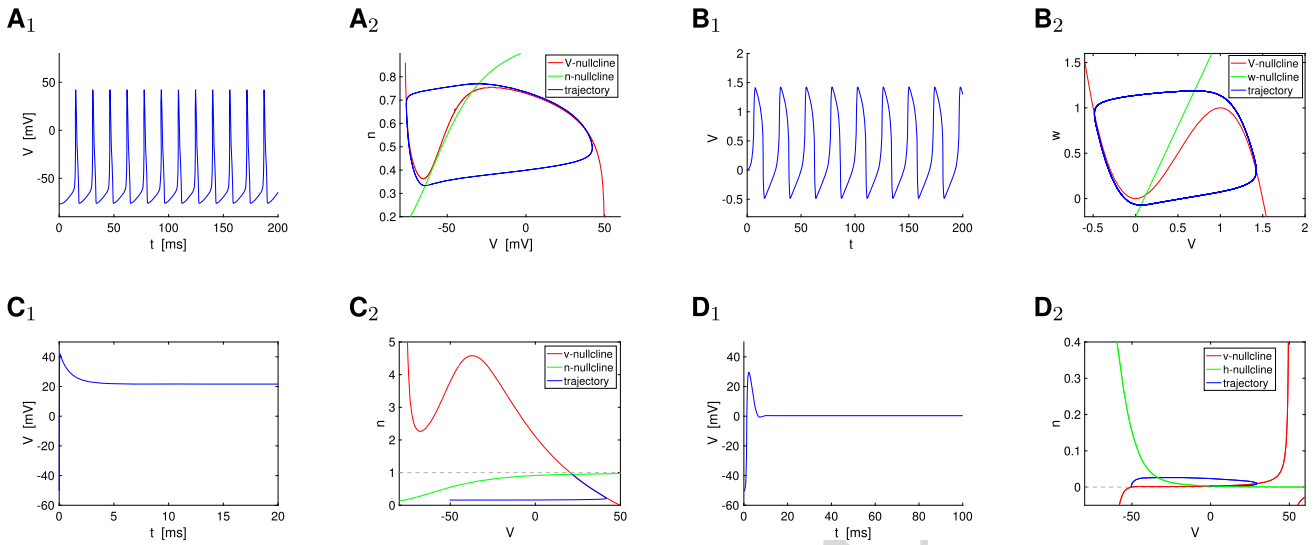

Fig. 6 Reduced and caricature models of neuronal activity. **A** Reduced (2D) HH model. The variable m in (1) was substituted by $m_\infty(V)$ and the variable $h = 1-\alpha\, n$ with $\alpha = 1.18$. The model captures the dynamics of the original HH model. **B** Phenomenological (caricature) model of FHN type. We used the following parameter values: $h = 2$, $a = 3$, $\alpha = 2$, $\epsilon = 0.1$ and $\lambda = 0.2$. **C** $I_{\rm Na}$+$I_{\rm K}$ reduced (2D) HH model. The variable m in (1) was substituted by $m_\infty(V)$ and the dynamics for h was eliminated from (1) (the variable h was substituted by $h = 1$). The trajectory starting at $V = E_L$ approaches a high voltage equilibrium. The model does not capture the dynamics of the original HH model. The cubic-like V-nullcline is present, but above the region of validity of n. The limit cycle ceases to be present as the result of the attempt to reduce the dimensionality of the model (making $h = 1$). **D** $I_{\rm Na}$ reduced (2D) HH model. The variable m in (1) was substituted by $m_\infty(V)$ and the variable n was eliminated from (1) ($G_K = 0$). The trajectory starting at $V = E_L$ approaches a high voltage equilibrium. The model does not capture the dynamics of the original HH model. The V-nullcline is no longer cubic-like. The limit cycle ceases to be present as the result of the attempt to reduce the dimensionality of the model (making $G_K = 0$). For the reduced HH models, we used the parameter values adapted (Ermentrout and Terman 2010) from the original model (Hodgkin and Huxley 1952a)

the spiking currents) and $V_{\rm thr}$ only indicates that a spike has occurred (soft threshold). In all these models, the spikes are all-or-non phenomena and their size is the same for all of them. We collectively refer to these models as models of IF type and add the dimensionality of the constituent (subthreshold) models of HH type (e.g., the LIF models are "1D linear models of IF type"). However, as noted above, the effective model dimensionality is higher. Other authors have referred to these models as generalized IF models (Jolivet et al. 2004; Richardson et al. 2003).

The models of IF type primarily solve two problems. First, their complexity is reduced as compared to the models of HH type that would be used to model the same phenomena or investigate the same theoretical problem. Second, the computational complexity is reduced since the elimination of the fast spiking dynamics (fastest time scales) eliminates the stiffness of system of differential equations.

In principle, one can construct models of IF type from models of HH type by leaving all the currents intact at the subthreshold voltage level and substituting the spiking dynamics by artificial spikes as described above. While in some cases, the spiking currents may be eliminated without major consequences for the dynamics (Rotstein et al. 2006), in others the elimination of the spiking currents at the subthreshold level may lead to qualitative dynamic changes (Jalics et al. 2010). One may then reduce the dimensionality of the models by using "top-down" approach described in Sect. 3. The resulting models may still be too complex for analysis.

The classical, "bottom-up" approach produces models of IF type with simpler low-dimensional subthreshold dynamics. Starting from the LIF model, the complexity and dimensionality of the model of IF type can be increased by adding nonlinearities to the current-balance equations and adding dynamic variables (e.g., recovery) to the system. The nonlinearities are typically idealized (e.g., parabolic, quartic, exponential), capturing the type of nonlinearities present in the V-nullclines (or nullsurfaces) in the phase-space diagrams (e.g., Figs. 6 and 7) for the more realistic models of HH type.

2D models of IF type are commonly referred to as "adaptive" for historical reasons. However, they capture neuronal phenomena that go well beyond adaptation.

7.2.1 Interpretability in terms of the biophysical properties of neurons

In order to make the results interpretable in terms of the biophysical properties of neurons, the parameter of the models

Journal: 422 MS: 0960 TYPESET DISK LE CP Disp.:2023/3/25 Pages: 21 Layout: Large

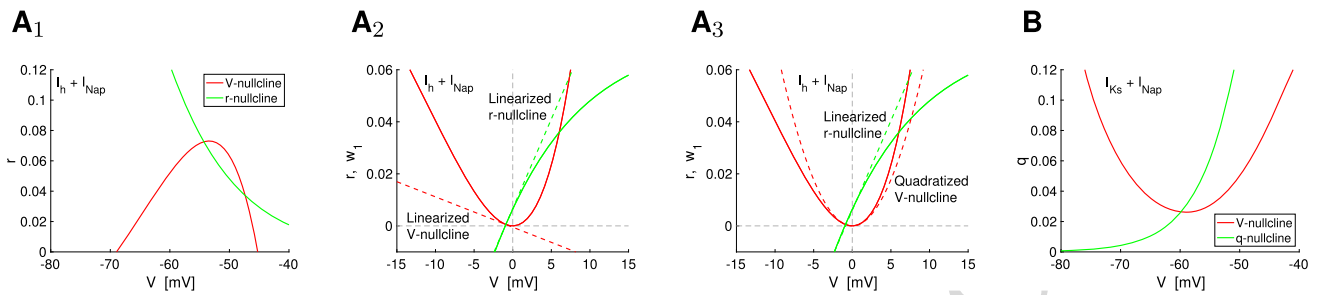

Fig. 7 Linearization and quadratization for models of HH type in the subthreshold voltage regime. **A** $I_h + I_{\text{Nap}}$ model. **B** $I_{\text{Ks}} + I_{\text{Nap}}$ model. The models are described by Eqs. (2)–(3). For the both models, the persistent Na current is described by $I_2 = I_{\text{Nap}} = G_p\, p_\infty(V)(V - E_{\text{Na}})$. For the $I_h + I_{\text{Nap}}$ model, the h-current (hyperpolarization-activated mixed Na/K) is described by $I_1 = I_h = G_h r(V - E_h)$ and for the $I_{\text{Ks}} + I_{\text{Nap}}$ model, the Ks-current (M-current) is described by $I_1 = I_{\text{Ks}} = G_q q(V - E_K)$. We used the same parameter values as in Turnquist and Rotstein (2018). The phase-plane diagrams present the relevant nullclines. The trajectories are omitted for clarity. $\mathbf{A}_a$ $I_h + I_{\text{Nap}}$ model with a parabolic-like nonlinearity. $\mathbf{A}_2$ Linearized $I_h + I_{\text{Nap}}$ model (see Sect. 6.1). The original (inverted) V and r-nullclines (solid) are presented for reference. The linearized V- and r-nullclines (dashed) are the v- and w_1-nullclines for the linearized system. $\mathbf{A}_3$ Quadratized $I_h + I_{\text{Nap}}$ model (see Sect. 6.2). The original (inverted) V and r-nullclines (solid) are presented for reference. The quadratized V- and linearized r-nullclines (dashed) are the v- and w_1-nullclines for the quadratized system. **B.** $I_h + I_{\text{Ks}}$ model with a parabolic-like nonlinearity

of IF type can be linked to the neuronal biophysical parameters by following the quadratization procedure described in Sects. 6.2. This process can be naturally extended to include higher dimensions and higher-order nonlinearities (e.g., cubization, quartization) by keeping more terms in the Taylor expansion of the V-nullcline and making the appropriate algebraic manipulations to simplify the resulting expressions.

7.2.2 Interpretability in terms of the observed neuronal patterns

The approach introduced in Fourcaud-Trocme et al. (2003) consists of a general formulation for the current-balance equation in the subthreshold regime

$$C\frac{\mathrm{d}V}{\mathrm{d}t} = -g_L(V - E_L) + \Psi(V; V_T, \Delta_T) + I_{\text{app}} \qquad (43)$$

where the parameters V_T and Δ_T of the nonlinear function Ψ are determined from the observed data (or modeling results using models of HH type) of the I–V curve.

The parameter V_T is defined as the value at which the slope of the I–V curve vanishes

$$\Psi'(V_T; V_T, \Delta_T) = g_L.$$

As such, it is the largest stationary value of V at which the neuron can be maintained by a constant current $I_T = g_L(V_T - E_L) - \Psi(V_T)$, above which the neuron exhibits tonic firing. The parameter ΔT (mV) is defined as

$$\Delta_T = \frac{g_L}{\Phi''(V_T)}.$$

It is called the spike slope factor and measures the sharpness of the spike initiation for reasons that will become clear later (see Naundorf et al. 2006; McCormick et al. 2007 for a discussion on the topic in biophysical models).

In order to make the models interpretable, the parameters V_T and Δ_T need to be estimated from the observed patterns one wants to model in advance of building the model since they are not linked to the constituent biophysical properties of neurons.

Similar to the models discussed in Sect. 6.2, this model can be augmented to include an adaptive process

$$C\frac{\mathrm{d}V}{\mathrm{d}t} = -g_L(V - E_L) + \Psi(V; V_T, \Delta_T) - w + I_{\text{app}} \qquad (44)$$

$$\tau_w\frac{\mathrm{d}w}{\mathrm{d}t} = a(V - E_L) - w \qquad (45)$$

The resulting 2D models were original built to capture the phenomenon of spike-frequency adaptation (e.g., by I_M). But the variable w can be interpreted to be any resonant gating variables (I_h, Ca inactivation).

An alternative approach has been developed in Kistler et al. (1997), Gerstner and Kistler (2002), Jolivet et al. (2004) based on Volterra expansions in the context of spike response models (SRMs).

7.3 2D (and 3D) linear models of IF type

These models extend the LIF model to include a recovery variable (Young 1937) interpreted as providing a negative feedback effect (e.g., I_h, I_{Ks}, I_{Ca} inactivation). However, in principle there is no reason why the recovery variable could not provide a positive feedback effect.

Journal: 422 MS: 0960 TYPESET DISK LE CP Disp.:2023/3/25 Pages: 21 Layout: Large

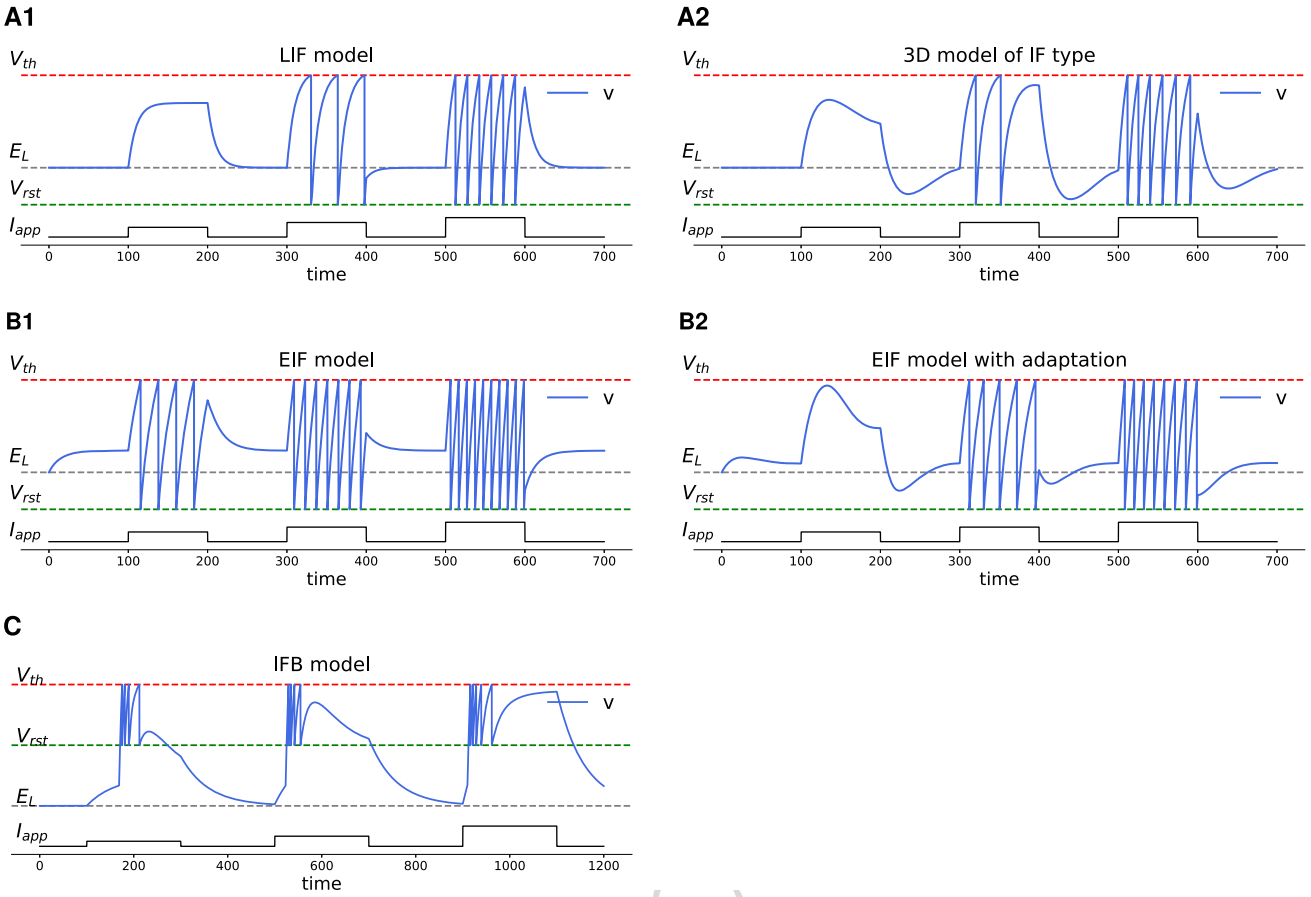

Fig. 8 Models of integrate-and-fire (IF) type: V-time course response to three consecutive square pulses with increasing amplitudes. **A1** Leaky IF (LIF) model. We used the following parameter values: $g_L = 0.1$, $E_L = 0$, $V_{\text{th}} = 5$ and $V_r = -2$. **A2** 3D linear model of IF type. The model includes two recovery variables (w_1 and w_2) interpreted as providing negative and positive feedback effects. The model is a 3D extension of Eqs. (26)–(27) (see Richardson et al. 2003; Rotstein 2017a). We used the following parameter values: $g_L = 0.1$, $E_L = 0$, $g_1 = 0.1$, $g_2 = -0.05$, $\tau_1 = 50$, $\tau_2 = 10$, $V_{\text{th}} = 5$, $V_{\text{rst}} = -2$. **B1** Exponential IF (EIF) model. The model is described by Eqs. (48). We used the following parameter values: $g_L = 0.1$, $V_{\text{th}} = 5$, $V_{rst} = -2$ and $\Delta_T = 2$. **B2** Adaptive EIF model. We used the same parameters as in panel B1 and $\tau = 50$ and $a = 0.1$ for the adaptive variable w. **C** Integrate-and-fire-or-burst (IFB) model. We used the following parameter values (see Smith et al. 2000): $C = 2$, $g_L = 0.035$, $E_L = -65$, $E_{\text{Ca}} = 120$, $V_{\text{th}} = -35$, $V_{rst} = -50$, $V_h = -60$, $g_T = 0.07$, $\tau_h^+ = 100$, $\tau_h^- = 20$. In $\mathbf{A}_1$, $\mathbf{A}_2$, $\mathbf{B}_1$ and $\mathbf{B}_2$ we used of $I_{\text{app},1} = 0.35$, $I_{\text{app},2} = 0.525$ and $I_{\text{app},3} = 0.7$ and the duration of step input was $\Delta = 100$. In **C** we used $I_{\text{app},1} = 0.0875$, $I_{\text{app},2} = 0.175$, $I_{\text{app},3} = 0.35$ and $\Delta = 200$

The subthreshold dynamics are described by a 2D linear system of the form (26)–(27) or, alternatively, (21)–(22). The mechanism of spike generation is determined by V_{thr}. The model parameters can be linked to biophysical parameters by the process of linearization of models of HH type described in Sect. 6.1. The models can produce spike-frequency adaptation (Treves 1993) (accommodation Hill 1936), subthreshold oscillations (Izhikevich 2001, 2006), subthreshold resonance and phasonance (Richardson et al. 2003; Rotstein and Nadim 2014; Rotstein 2014), post-inhibitory rebound, type II excitability, and are the substrate of complex phenomena such as hyperexcitability in recurrently connected networks (Rotstein 2013). We note that under certain conditions, the 2D models of IF type have been referred to as resonate-and-fire models (Izhikevich 2001, 2006)

3D (and higher-dimensional) linear models of IF type (e.g., Fig. 8-A2) can be obtained by generalizing the ideas discussed above and follow the linearization process (e.g., see Richardson et al. 2003; Rotstein 2017a). These models show additional phenomena such as antiresonance and antiphasonance (Richardson et al. 2003; Rotstein 2017a)

7.4 Quadratic IF model (QIF, 1D quadratic model of IF type)

The subthreshold dynamics for the (canonical) quadratic integrate-and-fire model (Latham et al. 2000) is described by

$$\frac{\mathrm{d}V}{\mathrm{d}t} = -V^2 + I_{\text{app}}. \tag{46}$$

Journal: 422 MS: 0960 TYPESET DISK LE CP Disp.:2023/3/25 Pages: 21 Layout: Large

The idealized parabolic nonlinearity is assumed to be an approximation to the parabolic-like nonlinearities present in neuronal models in vicinities of the resting potential, which develop due to the presence of regenerating (amplifying) currents such as I_{Na}. In fact, Eq. (46) is the topological form of a saddle-node bifurcation for 1D systems (Izhikevich 2006; Strogatz 1994) (see also Ermentrout and Kopell 1986 for a derivation and description of the related theta model). These geometric arguments can be made mathematically more precise and the results can be made interpretable by adapting the quadratization procedure described in Sect. 6.2.

For $I_{app} < 0$, Eq. (46) has two equilibria (V_{rest}, stable, and V_T, unstable), while for $I_{app} > 0$, there are no equilibria. Therefore, the QIF model describes the onset of spikes and V_{thr} only indicates the occurrence of a spike.

In terms of the formulation presented in Sect. 7.2, the QIF model reads (Fourcaud-Trocme et al. 2003)

$$C\frac{dV}{dt} = -g_L(V - E_L) + \frac{g_L}{2\Delta_T}(V - V_T)^2 - I_T. \qquad (47)$$

However, note that the quadratization process from models of HH type will produce an additional linear term not included in Eq. (47).

7.5 Exponential IF model (EIF, 1D exponential model of IF type)

The EIF model (Fig. 8-B1) uses a sharper nonlinearity in the current-balance equation than the QIF model (Fourcaud-Trocme et al. 2003)

$$\frac{dV}{dt} = -g_L(V - E_L) + g_L\,\Delta_T e^{\frac{V-V_T}{\Delta_T}} + I_{app} \qquad (48)$$

The EIF model has been shown to improve the accuracy of both the neuronal subthreshold and firing dynamics as compared to the model of HH type that would describe the same phenomenon.

7.6 Adaptive QIF models (2D quadratic model of IF type) and extensions (3D and higher, higher-order nonlinearities)

These model consists of adding a term $-w$ to Eq. (46) and a differential equation of the form (44) to the model (Izhikevich 2010, 2006). $\Psi(V; V_t, \Delta_T) = g_L(V - V_T)^2/(2\Delta_T)$ in Eqs. (44)–(45), which is the second term in the right-hand side in Eq. (47), (ii) Eqs. (23)–(24) in Sect. 5.5, and (iii) Eqs. (29)–(30) in Sect. 6.2. In all cases, V_{thr} is soft. These models exhibit a number of spiking and bursting patterns and subthreshold phenomena observed in realistic neurons. V_{rst} plays an important role in controlling the occurrence and properties of the bursting patterns (Izhikevich 2001).

2D models of IF type can be extended to higher dimensions either by deriving them from models of HH type, leading to Eqs. (40)–(42) (Turnquist and Rotstein 2018), or, simply, by "manually" adding another term (e.g., $-z$) to Eq. (46) and a differential equation to describe the dynamics of z. 2D models can also be extended to include higher-order nonlinearities, again, either by deriving them from HH models of HH type (including additional terms in the Taylor expansion of the current-balance equation) or, simply, by including them "manually" (e.g.,4D Touboul 2008). Higher order nonlinearities increase the sharpness of the V-nullcline (or nullsurface) and therefore control the properties of the subthreshold dynamics and the onset of spikes.

The 2D model of IF type used in Rotstein et al. (2006), Rotstein (2017a) where the subthreshold dynamics are described by a (biophysically plausible) reduced model of HH type having two active ionic currents (I_{Nap} and I_h) is a generalization of the adaptive QIF model where the V-nullcline is parabolic-like. However, a second model having exactly the same ionic currents, but in different parameter regimes, shows cubic-like nullclines (in the subthreshold regime). These are not the result of an extension of the quadratization process (cubization) described above, but inherent to the model. A similar scenario occurs for 2D models of IF type having an I_M instead of I_h.

7.7 Adaptive EIF models (AdEx, 2D exponential model of IF type) and extensions

These models could be included as extensions of the quadratic 2D models of IF type discussed above, but they deserve a special mention given its historic importance.

Adaptive EIF models (Fig. 8-B2) are obtained by adding a term $-w$ to Eq. (48) and a differential equation of the form (44) to the model (Brette and Gerstner 2005), thus increasing the dimensionality to 2D. An additional formulation consists of using $\Psi(V; V_t, \Delta_T) = g_L\,\Delta_T exp((V - V_T)/\Delta_T)$ in Eqs. (44)–(45), which is the second term in the right-hand side in Eq. (48).

The two extensions used in Barranca et al. (2013) consist of using explicit description of I_M and I_{AHP} instead of the term $-w$ in the current-balance equation. In the second case, a differential equation describing the dynamics of Ca concentration instead of a voltage-dependent gating variable was included in the model.

7.8 Integrate-and-fire-or-burst (IFB) model

This model was introduced in Smith et al. (2000) to investigate the mechanisms of post-inhibitory rebound bursting in thalamic relay cells and the transition from spike- to burst-

Journal: 422 MS: 0960 TYPESET DISK LE CP Disp.:2023/3/25 Pages: 21 Layout: Large

mode in these cells (Fig. 8-C). The subthreshold dynamics are described by

$$C\frac{dV}{dt} = -g_L(V - E_L) - g_T m_\infty(V)h(V - E_{Ca}) + I_{app},$$
$$\frac{dh}{dt} = \frac{1-h}{\tau_h^+}H(V_h - V) - \frac{h}{\tau_h^-}H(V - V_h). \quad (49)$$

The second term in the right-hand side in Eq. (49) is an idealization of I_{CaT} with $m_\infty(V) = H(V - V_h)$ where $H(\cdot)$ is the Heaviside function. The second equation describes the dynamics of an hyperpolarization-activated gating variable with $\tau_h^+ \gg \tau_h^-$ and $E_L < V_h < V_{thr}$.

8 Final remarks

Models of single neurons, and neuronal models in general, can be constructed in a variety of ways and at different levels of abstraction depending on the problem they are designed to solve. Single neuron low-dimensional models range from biophysically plausible (conductance-based) to phenomenological (caricature) descriptions, and can be systematically derived from higher dimensional models of HH type (using a variety of tools and approaches) or constructed ad hoc. In the former case, the link between the reduced models and the more realistic ones provides the reduced models and the results obtained by using them with a biophysical interpretation.

Models of single neurons are typically embedded in larger networks. In order to preserve the interpretability of neuronal network models, the network building blocks, particularly the single neuron model components and synaptic connectivity, must be compatible, or rules must be provided to create compatibility among the building blocks. This is particularly crucial when one uses reduced descriptions of single neurons (or other processes). In these cases, the systematic reductions should include the synaptic connectivity as opposed to synaptically connect reduced models.

Ultimately, neuronal models must be fit to experimental results. A number of parameter estimation tools are available to achieve this (Akman and Schaefer 2015; Brunton et al. 2016; Champion et al. 2019; Deb 2001; Deb and Beyer 2001; Deb et al. 2002a, b; Evensen 2009; Goncalves et al. 2020; Lillacci and Khammash 2010; Moye and Diekman 2018; Mensi et al. 2012; Papamarkou et al. 2019; Pozzorini et al. 2015; Rossi 2018; Shahriari et al. 2016; Senov and Granichin 2017; Walter and Pronzato 1997; Teeter et al. 2018; van Geit et al. 2008). In using parameter estimation tools (Mensi et al. 2012; Pozzorini et al. 2015; Teeter et al. 2018) one must take into account issues such as the variability of neuronal systems (Marder 2011; Taylor and Marder 2011), degeneracy (Edelman and Gally 2001; Goaillard and Marder 2021; Prinz et al. 2004) and unidentifiability (Lederman et al. 2022) (see references therein).

Acknowledgements The authors acknowledge support from the NSF Grants CRCNS-DMS-1608077 (HGR) and IOS-2002863 (HGR), from CONICET, Argentina (UC), and the Fulbright Program (VGB). The authors are thankful to John Rinzel for useful suggestions and discussions. This paper benefited from discussions held as part of the workshop "Current and Future Theoretical Frameworks in Neuroscience" (San Antonio, TX, Feb 4–8, 2019) supported by the NSF Grants DBI-1820631 (HGR) and IOS-1516648 (Fidel Santamaría, co-organizer). This paper also benefited from discussions during the course on "Reduced and simplified spiking neuron models" taught at the VIII Latin American School on Computational Neuroscience (LASCON 2020) organized by Antonio Roque (USP, Brazil) and supported by FAPESP Grants 2013/07699-0 (NeuroMat) and 2019/10496-0 and the IBRO-LARC Schools Funding Program. The authors are grateful to an anonymous reviewer for useful comments and suggestions.

Author Contributions HGR conceived the research and the manuscript. All authors wrote the main manuscript, prepared figures and reviewed the manuscript.

Declarations

Conflict of interest The authors declare no conflict of interest.

References

Abbott LF (1999) Lapicque's introduction of the integrate-and-fire model neuron (1907). Brain Res Bull 50:303–304

Acker CD, Kopell N, White JA (2003) Synchronization of strongly coupled excitatory neurons: Relating network behavior to biophysics. J Comput Neurosci 15:71–90

Akman O, Schaefer E (2015) An evolutionary computing approach for parameter estimation investigation of a model for cholera. J Biol Dyn 9:147–158

Baer SM, Erneux T, Rinzel J (1989) The slow passage through a Hopf bifurcation: delay, memory effects, and resonance. SIAM J Appl Math 49:55–71

Barranca VJ, Johnson DC, Moyher JL, Sauppe JP, Shkarayev MS, Kovacic G, Cai D (2013) Dynamics of the exponential integrate-and-fire model with slow currents and adaptation. J Comput Neurosci 37:161–180

Bertram R, Butte MJ, Kiemel T, Sherman A (1995) Topological and phenomenological classification of bursting oscillations. Bull Math Biol 57:413–439

Bonhoeffer K (1948) Activation of passive iron as a model for the excitation of nerve. J Gen Physiol 32:69–91

Borgers C (2017) An introduction to modeling neuronal dynamics. Springer

Brette R, Gerstner W (2005) Adaptive exponential integrate-and-fire model as an effective description of neuronal activity. J Neurophysiol 94:3637–3642

Brøns M, Kaper TJ, Rotstein HG (2008) Introduction to focus issue: mixed mode oscillations: experiment, computation, and analysis. Chaos 18:015101

Brunel N, van Rossum MCW (2007) Lapicque's 1907 paper: from frogs to integrate-and-fire. Biol Cybern 97:337–339

Brunton SL, Proctor JL, Kutz JN (2016) Discovering governing equations from data by sparse identification of nonlinear dynamical systems. Proc Natl Acad Sci USA 113:3932–3937

Journal: 422 MS: 0960 TYPESET DISK LE CP Disp.:2023/3/25 Pages: 21 Layout: Large

Burkitt AN (2006) A review of the integrate-and-fire neuron model: I. homogeneous synaptic input. Biol Cybern 95:1–19

Butera RJ, Rinzel J, Smith JC (1999) Models of respiratory rhythm generation in the pre-Botzinger complex. I. bursting pacemaker neurons. J Neurophysiol 82:382–397

Champion K, Lusch B, Kutz NJ, Brunton SL (2019) Data-driven discovery of coordinates and governing equations. Proc Natl Acad Sci USA 116:22445–22451

Coombes S, Bressloff PC (1999) Mode locking and arnold tongues in integrate-and-fire neural oscillators. Phys Rev E 60:2086–2096

Dayan P, Abbott LF (2001) Theoretical neuroscience. The MIT Press, Cambridge

Deb K (2001) Multi-objective optimization using evolutionary algorithms. Wiley, Hoboken

Deb K, Beyer H-G (2001) Self-adaptive genetic algorithms with simulated binary crossover. Evol Comput 9:197–221

Deb K, Anand A, Joshe D (2002) A computationally efficient evolutionary algorithm for real-parameter optimization. Evol Comput 10:371–395

Deb K, Pratap A, Agarwal S, Meyarivan T (2002) A fast and elitist multiobjective genetic algorithm: Nsga-ii. IEEE Trans Evolut Comput 6:182–197

Edelman GM, Gally JA (2001) Degeneracy and complexity in biological systems. Proc Natl Acad Sci USA 98:13763–13768

Ermentrout GB (1996) Type I membranes, phase resetting curves, and synchrony. Neural Comput 8:979–1001

Ermentrout GB, Kopell N (1986) Parabolic bursting in an excitable system coupled with a slow oscillation. SIAM J Appl Math 46:233–253

Ermentrout BG, Kopell N (1998) Fine structure of neural spiking and synchronization in the presence of conduction delays. Proc Natl Acad Sci USA 95:1259–1264

Ermentrout GB, Terman D (2010) Mathematical foundations of neuroscience. Springer

Evensen G (2009) Data assimilation: the ensemble Kalman filter. Springer

FitzHugh R (1960) Thresholds and plateaus in the Hodgkin-Huxley nerve equations. J Gen Physiol 43:867–896

FitzHugh R (1961) Impulses and physiological states in models of nerve membrane. Biophysical J 1:445–466

Fourcaud-Trocme N, Hansel D, van Vreeswijk C, Brunel N (2003) How spike generation mechanisms determine the neuronal response to fluctuating input. J Neurosci 23:11628–11640

Fransén E, Alonso AA, Dickson CT, Magistretti ME, Hasselmo J (2004) Ionic mechanisms in the generation of subthreshold oscillations and action potential clustering in entorhinal layer II stellate neurons. Hippocampus 14:368–384

Fuortes MGF, Mantegazzini F (1962) Interpretation of the repetitive firing of nerve cells. J Gen Physiol 45:1163–1179

Gabbiani F, Cox SJ (2017) Mathematics for neuroscientists, 2nd edn. Academic Press

Gerstner W, Kistler WM (2002) Spiking neuron models. Cambridge University Press

Gerstner W, Kistler WM, Naud R, Paninski L (2014) Neuronal dynamics: from single neurons to networks and models of cognition. Cambridge University Press

Goaillard JM, Marder E (2021) Ion channel degeneracy, variability, and covariation in neuron and circuit resilience. Annu Rev Neurosci 44:335–357

Golomb D (2014) Mechanism and function of mixed-mode oscillations in vibrissa motoneurons. PLoS ONE 9:e109205

Golomb D, Yue C, Yaari Y (2006) Contribution of persistent Na^+ current and M-Type K^+ current to somatic bursting in ca1 pyramidal cells: combined experimental and modeling study. J Neurophysiol 96:1912–1926

Goncalves PJ, Lueckmann J-M, Deistler M, Nonnenmacher M, Ocal K, Bassetto G, Chintaluri C, Podlaski WF, Haddad SA, Vogels TP, Greenberg DS, Macke JH (2020) Training deep neural density estimators to identify mechanistic models of neural dynamics. Elife 9:e56261

Hansel D, Mato G (2001) Existence and stability of persistent states in large neuronal networks. Phys Rev Lett 86:4175–4178

Hansel D, Mato G, Meunier C (1995) Synchrony in excitatory neural networks. Neural Comput 7:307–337

Hill AV (1936) Excitation and accommodation in nerve. Proc R Soc B 119:305–255

Hindmarsh JL, Rose RM (1994) A model for rebound bursting in mammalian neurons. Philos Trans R Soc Lond B 346:129–150

Hodgkin AL, Huxley AF (1952) A quantitative description of membrane current and its application to conductance and excitation in nerve. J Physiol 117:500–544

Hodgkin AL, Huxley AF (1952) Currents carried by sodium and potassium ions through the membrane of the giant axon of loligo. J Physiol 116:449–472

Hutcheon B, Yarom Y (2000) Resonance, oscillations and the intrinsic frequency preferences in neurons. Trends Neurosci 23:216–222

Izhikevich EM (2001) Resonate-and-fire neurons. Neural Netw 14:883–894

Izhikevich EM (2003) Simple model of spiking neurons. IEEE Trans Neural Netw 14:1569–1572

Izhikevich E (2006) Dynamical Systems in Neuroscience: the geometry of excitability and bursting. MIT Press, Cambridge

Izhikevich EM (2010) Hybrid spiking models. Philos Trans R Soc A 368:5061–5070

Jalics J, Krupa M, Rotstein HG (2010) A novel mechanism for mixed-mode oscillations in a neuronal model. Dyn Syst Int J 25:445–482

Johnston D, Wu SM-S (1995) Foundations of cellular neurophysiology. The MIT Press, Cambridge

Jolivet R, Lewis TJ, Gerstner W (2004) Generalized integrate-and-fire models of neuronal activity approximate spike trains of a detailed model to a high degree of accuracy. J Neurophysiol 92:959–976

Kass RE, Amari S-I, Arai K, Brown EN, Diekman CO, Diesmann M, Doiron B, Eden UT, Fairhall A, Fiddyment GM, Fukai T, Grün S, Harrison M, Helias M, Kramer MA, Nakahara H, Teramae J-N, Thomas PJ, Reimers M, Rodu J, Rotstein HG, Shea-Brown E, Shimazaki H, Shinomoto S, Yu BM (2018) Computational neuroscience: mathematical and statistical perspectives. Annu Rev Stat 5:183–214

Kepler TB, Marder E, Abbott LF (1990) The effect of electrical coupling on the frequency of model neuronal oscillators. Science 248:83–85

Kistler WM, Gerstner W, van Hemmen JL (1997) Reduction of the Hodgkin-Huxley equations to a single-variable threshold model. Neural Comput 9:1015–1045

Knight BW (1972) Dynamics of encoding in a population of neurons. J Gen Physiol 59:734–766

Koch C (1999) Biophysics of computation. Oxford University Press

Krupa M, Szmolyan P (2001) Relaxation oscillation and canard explosion. J Differ Equ 174:312–368

Lapicque L (1907) Recherches quantitatives sur l'excitation électrique des nerfes traitée comme une polarization. J Physiol Pathol Gen 9:620–637

Latham PE, Richmond BJ, Nelson PG, Nirenberg S (2000) Intrinsic dynamics in neuronal networks. I. Theory. J Neurophysiol 83:808–827

Lecar H (2007) Morris-lecar model. Scholarpedia 2:1333

Lederman D, Patel R, Itani O, Rotstein HG (2022) Parameter estimation in the age of degeneracy and unidentifiability. Mathematics 10:170

Levenstein D, Alvarez VA, Amarasingham A, Azab H, Gerkin RC, Hasenstaub A, Iyer R, Jolivet R, Marzen S, Monaco JD, Prinz A, Quarishi S, Santamaría F, Shivkumar S, Singh MF, Stockton DB, Traub R, Rotstein HG, Nadim F, Redish D (2020) On

Journal: 422 MS: 0960 ☐ TYPESET ☐ DISK ☐ LE ☐ CP Disp.:2023/3/25 Pages: 21 Layout: Large

the role of theory and modeling in neuroscience. arXiv preprint arXiv:2003.13825
Lillacci G, Khammash M (2010) Parameter estimation and model selection in computational biology. PLoS Comput Biol 6:e1000696
Manor Y, Rinzel J, Segev I, Yarom Y (1997) Low-amplitude oscillations in the inferior olive: A model based on electrical coupling of neurons with heterogeneous channel densities. J Neurophysiol 77:2736–2752
Marder E (2011) Variability, compensation, and modulation in neurons and circuits. Proc Natl Acad Sci USA 108:15542–15548
McCormick DA, Shu Y, Yu Y (2007) Hodgkin and Huxley model - still standing? Nature 445:E1–E2
Meng XY, Huguet G, Rinzel J (2012) Type III excitability, slope sensitivity and coincidence detection. Discrete Continuous Dyn Syst A 32:2729–2757
Mensi S, Naud R, Pozzorini C, Avermann M, Petersen CC, Gerstner J (2012) Parameter extraction and classification of three cortical neuron types reveals two distinct adaptation mechanisms. J Neurophysiol 107:1756–1775
Miller P (2018) An introductory course in computational neuroscience. MIT Press, Cambridge
Morris H, Lecar C (1981) Voltage oscillations in the barnacle giant muscle fiber. Biophysical J 35:193–213
Moye MJ, Diekman C (2018) Data assimilation methods for neuronal state and parameter estimation. J Math Neurosci 8:11
Nagumo JS, Arimoto S, Yoshizawa S (1962) An active pulse transmission line simulating nerve axon. Proc IRE 50:2061–2070
Naundorf B, Wolf F, Volgushev M (2006) Unique features of action potential initiation in cortical neurons. Nature 440:1060–1063
Papamarkou T, Hinkle J, Young JT, Womble D (2019) Challenges in Bayesian inference via markov chain monte carlo for neural networks. arXiv
Pena RFO, Rotstein HG (2022) Oscillations and variability in neuronal systems: interplay of autonomous transient dynamics and fast deterministic fluctuations. J Comput Neurosci
Perkel DH, Mulloney B, Budelli RW (1981) Quantitative methods for predicting neuronal behavior. Neuroscience 6:823–837
Pozzorini C, Mensi S, Hagens O, Naud R, Koch C, Gerstner W (2015) Automated high-throughput characterization of single neurons by means of simplified spiking models. PLoS Comput Biol 11:e1004275
Prescott SA, De Koninck Y, Sejnowski TJ (2008) Biophysical basis for three distinct dynamical mechanisms of action potential initiation. PLoS Comp. Biol. 4:e100198
Prescott SA, Ratté S, De Koninck Y, Sejnowski TJ (2008) Pyramidal neurons switch from integrator in vitro to resonators under in vivo-like conditions. J Neurophysiol 100:3030–3042
Prinz AA, Bucher D, Marder E (2004) Similar network activity from disparate circuit parameters. Nature Neurosci. 7:1345–1352
Prinz AA, Abbott LF, Marder E (2004) The dynamic clamp comes of age. Trends Neurosci 27:218–224
Richardson MJE, Brunel N, Hakim V (2003) From subthreshold to firing-rate resonance. J Neurophysiol 89:2538–2554
Rinzel J (1986) A formal classification of bursting mechanisms in excitable systems. In: Proceedeings of the international congress of mathematicians, pp 1578–1593
Rinzel J (1985) Bursting oscillations in an excitable membrane model. In: Sleeman BD, Jarvis RJ (eds) Ordinary and partial differential equations lecture notes in mathematics, vol 1151. Springer, Berlin, pp 304–316
Rinzel J (1985) Excitation dynamics: Insights from simplified membrane models. Fed Proc 44:2944–2946
Rinzel J, Ermentrout GB (1998) Analysis of neural excitability and oscillations. In: Koch C, Segev I (eds) Methods in neural modeling, 2nd edn. MIT Press, Cambridge, pp 251–292
Rossi RJ (2018) Mathematical statistics: an introduction to likelihood based inference. Wiley, New York
Rotstein HG, Nadim F (2020) Neurons and neural networks: computational models. In: Encyclopedia of life sciences. Wiley, Chichester
Rotstein HG (2013) Abrupt and gradual transitions between low and hyperexcited firing frequencies in neuronal models with fast synaptic excitation: A comparative study. Chaos 23:046104
Rotstein HG (2014) Frequency preference response to oscillatory inputs in two-dimensional neural models: a geometric approach to subthreshold amplitude and phase resonance. J Math Neurosci 4:11
Rotstein HG (2015) Subthreshold amplitude and phase resonance in models of quadratic type: nonlinear effects generated by the interplay of resonant and amplifying currents. J Comput Neurosci 38:325–354
Rotstein HG (2017) Spiking resonances in models with the same slow resonant and fast amplifying currents but different subthreshold dynamic properties. J Comput Neurosci 43:243–271
Rotstein HG (2017) Resonance modulation, annihilation and generation of antiresonance and antiphasonance in 3d neuronal systems: interplay of resonant and amplifying currents with slow dynamics. J Comput Neurosci 43:35–63
Rotstein HG (2017) The shaping of intrinsic membrane potential oscillations: positive/negative feedback, ionic resonance/amplification, nonlinearities and time scales. J Comput Neurosci 42:133–166
Rotstein HG (2018) Subthreshold resonance and phasonance in single cells: 2D models. In: Jaeger D, Jung R (eds) Encyclopedia of computational neuroscience: Springer Reference (www.springerreference.com). Springer, New York
Rotstein HG, Nadim F (2014) Frequency preference in two-dimensional neural models: a linear analysis of the interaction between resonant and amplifying currents. J Comput Neurosci 37:9–28
Rotstein HG, Oppermann T, White JA, Kopell N (2006) The dynamic structure underlying subthreshold oscillatory activity and the onset of spikes in a model of medial entorhinal cortex stellate cells. J Comput Neurosci 21:271–292
Rotstein HG, Wechselberger M, Kopell N (2008) Canard induced mixed-mode oscillations in a medial entorhinal cortex layer II stellate cell model. SIAM J Appl Dyn Syst 7:1582–1611
Rotstein HG, Coombes S, Gheorghe AM (2012) Canard-like explosion of limit cycles in two-dimensional piecewise-linear models of FitzHugh-Nagumo type. SIAM J Appl Dyn Syst 11:135–180
Senov A, Granichin O (2017) Projective approximation based gradient descent modification. IFAC-PapersOnLine 50:3899–3904
Shahriari B, Swersky K, Wang Z, Adams RP, de Freitas N (2016) Taking the human out of the loop: a review of Bayesian optimization. Proc IEEE 104:148–175
Sharp AA, O'Neil MB, Abbott LF, Marder E (1993) The dynamic clamp: artificial conductances in biological neurons. Trends Neurosci 16:389–394
Sharp AA, O'Neil MB, Abbott LF, Marder E (1993) Dynamic clamp: computer-generated conductances in real neurons. J Neurophysiol 69:992–995
Smith GD, Cox CL, Sherman SM, Rinzel J (2000) Fourier analysis of sinusoidally driven thalamocortical relay neurons and a minimal integrate-and-fire-or-burst model. J Neurophysiol 83:588–610
Stein RB (1965) A theoretical analysis of neuronal variability. Biophysical J 5:173–194
Stein RB (1967) Some models of neuronal variability. Biophysical J 7:37–68
Strogatz SH (1994) Nonlinear dynamics and Chaos. Addison Wesley, Reading MA
Szmolyan P, Wechselberger M (2001) Canards in r^3. J Differ Equ 177:419–453
Taylor AL, Marder E (2011) Multiple models to capture the variability in biological neurons and networks. Nat Neurosci 14:133–138

Journal: 422 MS: 0960 ☐ TYPESET ☐ DISK ☐ LE ☐ CP Disp.:2023/3/25 Pages: 21 Layout: Large

Teeter C, Iyer R, Menon V, Gouwens N, Feng D, Berg J, Szafer Z, Cain H, Zeng N, Hawrylycz M, Koch C, Mihalas S (2018) Generalized leaky integrate-and-fire models classify multiple neuron types. Nat Commun 9:709

Torben-Nielsen B, Segev I, Yarom Y (2012) The generation of phase differences and frequency changes in a network model of inferior olive subthreshold oscillations. PLoS Comput Biol 8:31002580

Touboul J (2008) Bifurcation analysis of a general class of nonlinear integrate-and-fire neurons. SIAM J Appl Math 68:1045–1079

Treves A (1993) Mean-field analysis of neuronal spike dynamics. Network 4:259–284

Tuckwell HC (1988) Introduction to theoretical neurobiology, vol 2. Cambridge University Press

Turnquist AGR, Rotstein HG (2018) Quadratization: from conductance-based models to caricature models with parabolic nonlinearities. In: Jaeger D, Jung R (eds) Encyclopedia of computational neuroscience. Springer-Verlag, New York

van der Pol B (1920) A theory of the amplitude of free and forced triode oscillations. Radio Rev 1(701–710):754–762

van Geit W, De Schutter E, Achard P (2008) Automated neuron model optimization techniques: a review. Biol Cybern 99:241–251

Walter E, Pronzato L (1997) Identification of parametric models from experimental data. Springer, London

Wang X-J, Buzsáki G (1996) Gamma oscillations by synaptic inhibition in an interneuronal network model. J Neurosci 16:6402–6413

Wang X-J, Rinzel J (1992) Alternating and synchronous rhythms in reciprocally inhibitory model neurons. Neural Comput 4:84–97

Wechselberger M (2005) Existence and bifurcation of canards in R^3 in the case of a folded node. SIAM J Appl Dyn Syst 4:101–139

Young G (1937) Note on excitation theories. Psychometrika 2:103–106

Journal: **422** MS: **0960** ☐ TYPESET ☐ DISK ☐ LE ☐ CP Disp.:**2023/3/25** Pages: **21** Layout: **Large**

Journal: 422
Article: 960

Author Query Form

Please ensure you fill out your response to the queries raised below and return this form along with your corrections

Dear Author

During the process of typesetting your article, the following queries have arisen. Please check your typeset proof carefully against the queries listed below and mark the necessary changes either directly on the proof/online grid or in the 'Author's response' area provided below

Query	Details required	Author's response
1.	As keywords are mandatory for this journal, please provide 3-6 keywords.	
2.	Please check and confirm the inserted city name of the affiliations is correct.	
3.	Please check and confirm the part label of Figures 6 and 7.	